PHOTOCONDUCTIVITY IN SEMICONDUCTING DIAMONDS AT LOW TEMPERATURES

By

JEFFERSON BRYAN KRUMME

Bachelor of Science
Oklahoma State University
Stillwater, Oklahoma
1958

Master of Science
Oklahoma State University
Stillwater, Oklahoma
1960

Submitted to the Faculty of the Graduate School of
the Oklahoma State University
in partial fulfillment of the requirements
for the degree of
DOCTOR OF PHILOSOPHY
May, 1965

PHOTOCONDUCTIVITY IN SEMICONDUCTING DIAMONDS

AT LOW TEMPERATURES

Thesis Approved:

William J. Lewis
Thesis Adviser

Robert Dreeman

Francis C. Todd

E. E. Kohnke

H. Harrington

J. J. Boggs
Dean of the Graduate School

ACKNOWLEDGEMENTS

The assistance of many people was gratefully received during this work. In particular, I want to express my gratitude to Dr. W. J. Leivo for the opportunity to do this work and for many stimulating discussions which always sought to uncover the basic principles involved in the problems we considered. I have benefitted also from discussions with Dr. H. E. Harrington, Dr. F. C. Todd, Dr. E. E. Kohnke, and Dr. R. D. Freeman each of whom has given me valuable guidance and counsel.

For making the diamonds available to the group at Oklahoma State University I wish to thank Dr. J. F. H. Custers of the Diamond Research Laboratory and Dr. G. Switzer of the U. S. National Museum.

The technical advice of H. D. Adams and B. J. Cottongim of Texas Instruments Company was immensely helpful in solving some measurement problems. Dr. S. Zwerdling of the Massachusetts Institute of Technology graciously provided me with a schematic of his dynamic follower circuit and discussed its use with me. I wish to thank each of these people.

The members of the Physics-Chemistry shop and the Chemistry glass shop were very helpful in both the design and construction of several pieces of equipment, many times under less than ideal scheduling situations, and I wish to thank them sincerely.

Finally, I gratefully acknowledge the financial support administered through the Research Foundation of Oklahoma State University.

TABLE OF CONTENTS

LIST OF TABLES

LIST OF FIGURES

CHAPTER I

INTRODUCTION

Statement of the Problem

The relative photoconductive response of semiconducting diamonds as a function of the wavelength of the incident radiation has been measured at crystal temperatures of 4.2°K and 77°K. The room temperature response was also obtained for comparison purposes. The data provide new information regarding the imperfections in this type of diamond and in addition provide a means of observing other crystal processes which may not be observable by less sensitive means.

In the present chapter a brief discussion of diamonds and a survey of diamond research is given. This will include the bulk of the previous work on photoconductivity in diamonds. Chapter II provides an introduction to the photoconductive process and definitions of terms. A theoretical treatment of photoconductivity is given as it applies to semiconducting diamonds. Chapter III contains a discussion of the experimental problem and the instrumentation which was developed. In Chapter IV the experimental data are presented and a discussion of the data is given.

Diamonds and Previous Diamond Research

Physical Description

Diamond is a crystalline substance composed of carbon atoms in a tetrahedral arrangement. The diamond structure can be represented by two face centered cubic lattices with corresponding lattice vectors parallel and one lattice displaced one-fourth of the way along a cell diagonal with respect to the other (1). Each carbon atom is thus surrounded by four other carbon atoms in a covalent bonding arrangement wherein all valence electrons are shared in pairs. This stable structure produces the hardest known natural material, and from the point of view of the crystallographer it should be optically isotropic (2). The crystal structure produces a very good insulator since the pairing of electrons fills the valence bands (3).

Early Investigations and Classification

The great interest in the study of diamonds is indicated by the growing bibliography of over four hundred papers regarding diamonds which has been compiled by the Oklahoma State University group headed by Professor W. J. Leivo. The bibliography does not include books or papers emphasizing the use of diamonds. Since the diamond lattice is the prototype for silicon, germanium and gray tin, it is to be expected that the technological push for understanding of silicon and germanium would stimulate a large interest in diamond.

The study of diamond predates interest in silicon and germanium. The work of Robertson, Fox, and Martin (4,5) mentions many of the earlier investigations and points out some discrepancies recorded regarding

optical absorption. Due to this lack of agreement those authors extended their study to include infrared spectroscopy "with the object of throwing more light on the (reflection and absorption) band structure, and if possible getting some interpretation of it." They probably intended no pun in that sentence and indeed, they succeeded in throwing a good bit of light on the optical absorption band structure.

They showed that some diamonds had "extra" absorption in the 8 μ spectral region and that these diamonds become opaque at about 0.3 μ. Other diamonds, vastly more rare, which failed to show definite optical absorption bands "even of small intensity" in the 6 μ to 17 μ spectral range were found to transmit to about 0.225 μ. They called the first group type I and the more transparent group type II. A general review of their papers is not intended, but it seems worthwhile to state a few of their findings. Type II diamonds tend to have a lamellar structure. On page 496, they list four "new" effects peculiar to diamonds of type II (4). "Production of a current on illuminating diamond with ultra-violet light of short wave-length without an applied field. Activation of diamonds by short wave length-light (about λ 2300) leaving dark current and subsequent increased response to light of longer wave-length. Removal of activation (deactivation) due to λ 2300 by light of wave-length λ 2400 to λ 5000. Large photo-conductivity when light of wave-length greater than λ 5000 is applied to activated but not to a deactivated diamond. (Region of adjuvant effect)." Diamonds of type I in general possess small photoconductivity even with quite large electric fields applied to the crystal.

A major discovery in the history of diamonds was made by Custers (6) who, in the course of a research program on type I and type II

diamonds, found a specimen which showed a strong blue phosphorescence and high conductivity when excited by ultra-violet radiation. A spectrum of the phosphorescence showed a broad continuous band with relative maxima at 4665, 5310 and 5720 Å. The peak at 4665 Å was the strongest, and this explained the blue color observed. Subsequently he presented a table of some properties of 21 such diamonds (7). All were light blue in color, were electrical conductors and to a varying extent they phosphoresced when irradiated with far ultra-violet radiation. Custers felt inclined to assume the conductivity to be a structural property rather than due to an impurity element. Since this new type of diamond was much like type II, Custers proposed that it be classed type IIb, and this has been generally accepted.

Leivo and Smoluchowski (8) found that type IIb diamond behaves like an impurity activated semiconductor with the value of the slope of k log ρ versus 1/T equal to 0.35 ev at room temperature. Using resistivity and Hall coefficient measurements between -40°C and 60°C Brophy (9) deduced an activation energy of 0.35 ev.

Oklahoma State University Diamond Research

The investigation of semiconducting diamonds at Oklahoma State University under the direction of W. J. Leivo was begun during this period. A comprehensive study of a few specimens was planned with the hope of overcoming the difficulties one encounters when trying to correlate published data which often are obtained from various specimens with unknown and diverse properties. Some of the results of these investigations will be given, but first it is desirable to identify the crystals used in the present work.

All specimens are semiconducting diamonds. DS-1 is a blue irregular chip, somewhat cigar shaped, with one end larger than the other. It has some flat cleavage faces of small area. DS-2 is a rectangular parallelepiped 2.5 x 3.5 x 6.5 mm^3 in size. One end of this diamond is blue, the color extending about 1/4 the length of the crystal. The rest of the specimen is water white. DS-3 is a large blue marquise cut diamond, and DS-6 is a smaller blue marquise cut specimen. The other diamonds in the collection will not be described here, but some of the results of previous investigations will now be given.

Extra optical absorption peaks typical of type IIb diamonds were found at 2.43, 3.40, 3.56 and 4.07 μ (10, 11, 12). In a study of electrical and optical properties of a semiconducting diamond, Austin and Wolfe (13) recorded extra infrared absorption as follows. A prominent peak at 3.57 μ and smaller peaks at 4.1 μ, 3.4 μ and 2.5 μ, and a continuum of absorption from 1 to 2.5 μ. The extra absorption was reversibly temperature dependent and was undetectable above 300°C. They mentioned a low resolution study at -155°C of the photoconductivity but did not publish a spectrum. A study by Clark, Ditchburn, and Dyer (14) gave essentially the same peaks but listed further absorption at 1.85, 2.35, and 4.23 μ. A very strong CO_2 atmospheric absorption occurs from 4.2 to 4.4 μ, and more will be said about it later.

The photovoltaic effect was studied at room temperature, and the photo-voltage was a maximum at 0.44 μ with a relative maximum at 0.66 μ and a weak one at 0.89 μ (12, 15). Photoconductive studies were made in the temperature range from room temperature to 127°K (11, 12, 16). Photoconductivity in the ultraviolet spectral region begins at about

0.236 μ (5.25 ev) and increases toward shorter wave lengths. Maxima were near 0.224 and 0.228 μ. From this range to about 0.350 μ no photoconductivity was found. A broad photoconductive band appeared from 0.35 to about 1.8 μ in the earliest investigation at room temperature, and a more detailed study was made. The data are summarized in Table I wherein the photoconductive maximum for each temperature is underlined. The 0.44 photovoltaic maximum was not recorded in the photoconductive investigations.

Hall studies verified the p type conductivity of the diamonds and yielded a mobility μ_H for holes of 1300 cm^2/volt sec. (12). Assuming a particular model, the effective hole mass of 0.3 m_e was found and an acceptor density of 3.25×10^{16} and donor density of 9.5×10^{15} were found to fit the theoretical curve.

Carrier lifetime measurements showed the complexity of the problem in diamond (11, 12, 17). A lifetime of 9 μ sec. was obtained for a diamond DS-2. This value is thought to be largely independent of trapping. Decay times obtained with various exciting wavelengths are 1/4 and 30 sec. and 6, 7, 12, 30, 39, and 84 minutes.

Luminescence investigations showed that the temperature dependence of the afterglow was that expected of phosphorescence rather than slow fluorescence (11, 18), and an indication of multiple metastable levels was found in the variation of intensity with temperature. A previously unreported red phosphorescence was found which varied in intensity between specimens DS-1, DS-2 and DS-3. It appeared stronger in the blue end than in the clear end of DS-2.

Electron spin resonance studies have led to the following conclusions (20). The spin resonance absorption is associated with the

TABLE I

SOME PROPERTIES OF DIAMOND

Property	Method	Diamond Type	Temperature	Reference
Activation Energy (ev)				
0.35	Resistivity	IIb	Room	(8)
0.35	Hall Effect	IIb	-40°C to +60°C	(9)
.22, .30, .38	Resistivity	IIb	125°K to 420°K	(21)
.21, .3, .37, .52, .7	Thermoluminescence glow	IIb	20°C to 100°C	(21)
Dielectric Constant				
5.66 (700 cps)	Method of Mixtures		27.8°C	(44)
5.68 $\pm$ 0.03 (500-3000 cps)	Method of Mixtures		Room	(44)
Density (gm/cm^3)				
3.515 typical	(see reference)	IIb	Room	(34)
Density of Impurities				
$N_A = 3.25 \times 10^{16}$	Hall Effect			
$N_D = 9.5 \times 10^{15}$	Hall Effect	IIb	Room	(12)
$(N_A - N_D)$ 4×10^{14} (DS-2)	esr			
$(N_A - N_D)$ 5×10^{13} (DS-1)	esr	IIb	Room	(19)
Effective Mass (hole) m^*_h/m_e				
2.12, 1.06, 0.7	Millimeter Cyclotron Resonance	IIb	4.2° and	(30, 31)
0.3	Hall Effect	IIb	1.2° K	(12)
Lifetime				
4 μ sec rise, 1/4 sec decay	Spark source	IIb	Room	(12)
6, 7, 12, 30, 39, 84 min.	Monochromator and Shutter	IIb		(12)

Property	Method	Diamond Type	Temperature	Reference
Mobility				
μ_h - 1300 cm^2/volt sec	Hall Effect	IIb		(12)
1400 cm^2/volt sec		IIb		(13)
1200, $\mu_h \propto T^{-3/2}$	Insulating	Insulating		
μ_e - 1800 ($\pm$20%), $\mu_e \propto T^{-3/2}$	Insulating	Insulating		(32)
Optical Absorption				
Extra Infrared Peaks (microns)				
2.43, 3.4, 3.56, 4.07		IIb	Room	(12)
Similar plus 1.85, 2.35, 4.23		IIb		(14)
1.85, 2.35, 2.43, 3.4, 3.58 4.05, 6, 6.2		IIb		(21)
Common to All				
2.64, 2.77, 3.16, 4.03, 4.65		II, IIa, IIb		(4)
Phosphorescence Maxima (microns)				
0.4665, 0.5310, 0.5720		IIb	Room	(6)
Photoconductivity Peaks (microns)				
.224, .228, .6, 1.46, 1.75		IIb	Room	(12)
.59			250°K	
.58 weak 1.24, 1.84, 2.02			223°K	
.052 .92, 1.6, 2.16			150°K	
.88			127°K	
See Chapter IV for present results		IIb	77°K, 4.2°K	
Recombination Radiation				
5.278 ev (0.234 μ), 5.125 ev (0.242 μ)	Carrier Injection	Insulating		(43)

acceptor center in p-type diamonds. The acceptor center is probably associated with a vacancy. The acceptor defects are distributed in thin layers that lie on (111) planes with concentrations possibly as high as 10^{21} per cc. Exchange interactions between acceptors is possible because of the compensation of acceptors. Colored diamonds usually have complicated spin resonance spectra.

Results of Investigation by Others

The extent of the literature on diamonds has been indicated earlier, and no survey will be attempted here. A few works of interest to the present writing will be selected for discussion.

A luminescent recombination process with quite broad spectral distribution has been reported (21). Halperin and Nahum show electroluminescent and fluorescent curves to be essentially identical with maximum at 0.47 μ. Unfortunately their data are uncorrected for change of their detector sensitivity with wave length. Wolfe and Woods (22) photographed the electroluminescence spectrum of diamond and show the peak intensity at 0.44 μ. The latter value is that of the photovoltaic maximum observed in this laboratory.

The temperature dependence of the dark conductivity of semiconducting diamond was extended to cover the temperature range 100°K to about 400°K by Halperin and Nahum (21). These measurements indicated additional activation energies of 0.22 and 0.30 ev and show 0.38 ev in the higher temperature range (280° to 420°K) instead of the previously reported 0.35 ev. Measurements on a second specimen yielded 0.20 and 0.29 ev activation energies. Contact failure caused the room temperature data to be discarded for this specimen. These investigators obtained a photoconductive spectrum in the spectral range 0.20 to

0.23 μ. They observed photoconductivity between 1 and 4 μ, but were unable to record the spectrum due to technical difficulties. Activation energies which they obtained from thermoluminescence glow curves agreed with those obtained from dark conductivity and provided two additional values of 0.52 evand 0.7 ev. These all are correlated with optical measurements in the infrared.

Male (23) measured the luminescence excitation spectrum for the three types of diamond. Whereas the excitation spectrum for type I, type IIa and an "intermediate" type showed bands, the semiconducting, type IIb, diamond showed a broad excitation spectrum beginning at 5.25 ev. The maximum is near 5.6 ev, and there is a peak at 5.5 ev which is the only feature which is possibly common to all diamond types.

Male and Prior (24) have observed intrinsic recombination radiation in a type IIa diamond utilizing carrier injection to provide the electron density required in order to make this improbable process measureable. They recorded a strong radiant peak at 5.278 ev and another about 1/4 as intense at 5.127 ev. The maximum energy of the radiant emmission was at 5.6 ev. The 5.278 ev peak was of the order of 0.1 per cent as intense as the maximum of the 4400A blue luminescent band. No attempt was made to assign phonon energies to the transitions recorded.

Some infrared absorption bands between 2.5 and 6 μ are common to all diamonds and have relative maxima near 2.64, 2.77, 3.16, 4.03, 4.6, and 5 μ according to Robertson, Fox, and Martin (4). Collins and Fan (25) who were investigating the lattice absorption bands in germanium and silicon found that the temperature dependence of the two bands near 4.8 μ suggested these were characteristic of the lattice. Assuming that the dipole moment of a lattice mode is proportional to the

root-mean-square thermal displacement and that the absorption is proportional to the mean square thermal displacement, they were able to compare the change in absorption with temperature to a theoretical curve by Lonsdale (26). The curve calculated by Lonsdale showed that the mean square thermal displacement of atoms in diamond was a slowly changing function of temperature and was small compared to silicon and germanium at room temperature. This is explained as resulting from the high Debye temperature (2340°K) of diamond.

In order to make the change in absorption with temperature observable, Collins and Fan made measurements at high temperatures. The result corresponded well with the theoretical expression. They found that the frequency 2175 cm^{-1} of the strong 4.6 μ absorption band in diamond was in good agreement with a theoretical expression relating lattice elastic constants and the limiting lattice vibration frequency. Since the Raman frequency in diamonds is 1332 cm^{-1} this implies that combination modes are involved. It appears that the 4.6 μ absorption is associated with an optical mode phonon. Lax and Burstein (27) suggested that in diamond type crystals, wherein a linear electric moment is absent, the infrared lattice absorption must involve charge deformation. Specifically one acoustic and one optical phonon are required for photon absorption. These phonons need to be short wave length modes to provide the required asymmetric displacement within the two sub-lattices of diamond. The two phonon idea was investigated further by Hardy and Smith (28) who made two proposed phonon energy assignments. They related the phonon assignments to the infrared absorption which they obtained at high resolution in order to make precise assignments possible. The results of their measure-

ments show relative maxima in the absorption constant for diamond to exist at 0.244, 0.251, 0.267 and 0.302 ev and with shoulders at 0.281 and 0.319-0.315 ev. They were unable to make a choice between their two proposed assignments on the basis of existing knowledge. Hardy, Smith, and Taylor (29) have observed phonon effects at 80°K in the "remarkably strong photoconductivity" of two semiconducting diamonds. The data cover the spectral range from about 1.4 to 3.4 μ. They relate phonon interactions to excited states of the 0.35 ev acceptor to explain their data and find evidence of three-phonon processes.

Rauch (30, 31) performed cyclotron resonance experiments on semiconducting diamond at 70 GHz and liquid helium temperatures. Monochromatic carrier excitation was used to obtain the resonance intensity as a function of the photon energy and phonon effects were also observed in his data. Rauch obtained 0.355 ev for the activation energy and 0.006 ev for the spin-orbit splitting energy in these crystals. He obtained hole effective masses 2.12, 1.06 and 0.7 for the three valence bands; the least value is for holes in the split-off band. A theoretical study by Birman (33) indicates that there are at least eleven different phonon frequencies to be assigned in a diamond structure material and possibly the correct number is 17.

A recent high precision study of the density of natural diamonds shows that type IIb semiconducting diamonds are less dense than type IIa or type I diamonds (34). This is in keeping with the suggestion that lattice vacancies may be the cause of p-type conductivity in semiconducting diamond (20).

Charette (35, 36) has made a low temperature study of the infrared absorption bands of diamond. He was able to record fine structure in

the 3.4 and 3.57 μ bands in semiconducting diamond. He found little change in these absorption features upon reducing the sample temperature from 77°K to 4.2°K except that two features disappeared. These were absorptions at 2755 and 2870 cm^{-1} corresponding to 3.630 and 3.484 μ respectively.

A large number of important studies have been omitted from this survey, and no suggestion is intended that they are less important. The work discussed above is of special interest to the present investigation.

CHAPTER II

PHOTOCONDUCTIVITY

Preliminary Remarks

The phenomenon has been known for such a long time that it is rather surprising that only a very few books have been written about photoconductivity. The converse is the case with journal papers. The photoconductive phenomenon has been widely studied and discussed in the literature since the first report in 1873 by W. Smith (37) who observed that the resistance of a selenium resistor in the daylight was not the same as it was in the dark. A book by Bube (38) is rather extensive and gives many references to the literature on photoconductivity. The recent book by Rose (39) in the author's words "stresses primarily a compact treatment of the concepts and formalisms I have found useful for understanding recombination processes, the interaction between space charge limited and photocurrents, the role of electrical contacts, and noise properties of currents in solids."

Photoconductivity is the increased conductivity of a substance due to its exposure to radiation. The spectral range currently being covered by commercially available photoconducting solids includes wave lengths from approximately 0.4 to 40 μ. Photoconductivity also includes the increased conductivity caused by ultra-violet, x, and γ rays and should in principle include excitation by particles such

as electrons, α-particles, β-rays or other nuclear radiation (40). The treatment of photoconductivity to be given here largely follows that of Rose (39, 40) and the extended treatment by Bube (38) with special points of interest drawn from wherever the writer finds source or perspective.

Gudden and Pohl (38) divided photoconductive materials into two classes. Idiochromatic materials showed photoconductivity in the pure state and in present day terminology would be called intrinsic photoconductors. Intrinsic implies the photoconductivity is a property of the pure material. The allochromatic class corresponds to extrinsic or impurity photoconductors. Absorption by F-centers in alkali halides has an associated photoconductivity. Gudden and Pohl distinguished between primary photocurrents which are due to photon absorption and secondary photocurrent due to passage of primary current. The primary current was numerically equal to the current of absorbed photons and secondary currents exceeded the current of absorbed photons. In this way the quantum nature of the excitation process was identified, but this point of view did not add to the understanding of the photoconductive process (40).

Photoconductivity in Solids

Distinction Between Insulators and Semiconductors

It is useful to provide some definitions and a background for the following description of photoconductivity. Since some diamonds are insulators and others are semiconductors it is believed that this difference should first be treated.

From the band theory of solids one obtains the following information regarding electron energies in a crystalline material (41). For

every state of an electron in the free atom there exists a band of energies in the crystal. The breadth of a band will be greater the more the atomic wave functions overlap. The number of states in a nondegenerate band is equal to the number N of atoms in the crystal and two electrons of opposite spin fill each state so that a full band contains 2N electrons. The energy within a band is a periodic function of the electron wave vector k so that $\nabla_k E$ must be zero at the edge of the Brillouin zone. The bands may be separated by bands of forbidden energy or may overlap for some values of the wave vector k. These are the results of the one electron theory wherein Bloch functions are used to obtain solutions to the appropriate Schrödinger equation. Further details are given in various books on the theory of solids (1, 3, 41, 42). The bands corresponding to inner core electrons are usually narrow and not of much interest in solids. The bands corresponding to the atomic valence electrons are the ones which have greater overlapping of wave functions, and they determine the interesting properties of the crystal. If the band of greatest energy which contains any electrons is full and is separated by a forbidden energy gap E_g from the next highest band, which is empty, there can be no change in the electron velocity distribution within the band upon application of an electric field, and the crystal is therefore an insulator. If the band is partly full or if an empty band overlaps a full band one has a metal. This case will not be considered further. Diamond has three valence bands which have maxima at the center of the Brillouin zone, k = 0. Two are degenerate at that point, the third band edge is split off by 0.006 ev due to spin orbit interaction. The measured effective hole masses are 2.12, 1.06 and 0.7 free electron masses m_e,

and correspond to three valence bands in order of decreasing electron energy. The third band is spherical and the upper two bands are nearly spherical. Only a 0.1 m_e variation in the heavy hole mass is indicated. These results were obtained from millimeter cyclotron resonance measurements at 1.55°K by C. J. Rauch (30, 31). The conduction band minima in diamond are neither at the center nor the edge of the Brillouin zone but are found at about 95 per cent of the distance to the edge of the Brillouin zone along the (1,0,0) axes (43). Since the conduction band is empty and separated by about 5.5 ev from the valence band, diamond is an insulator in its ideal form.

The above concept has not provided for a material to have properties between those of perfect insulators and the metallic conductors. The introduction of quantum statistics provides for conduction by an "insulator" without introducing lattice imperfections. They will be discussed later. The result of applying Fermi-Dirac statistics to the above picture is that there are always some electrons in the conduction band at any crystal temperature above 0°K. The electron density for a solid with a parabolic band wherein $E \propto k^2$ is given by

$$n = 2(2\pi m^* kT/h^2)^{3/2} \exp\left[(E_f - E_c)/kT\right] \qquad (2.1)$$

In this expression m* is the density of states effective mass, h is Plancks constant, k is Boltzmann's constant, T the absolute temperature, E_c the electron energy at the conduction band minimum, and E_f is the Fermi energy.

Thus since T = 0 is thermodynamically prohibited, the concept of a perfect insulator is invalid. Nature provides "good" and "bad" conductors of electricity. The above expression will be evaluated for

"pure" diamond at 300°K to provide insight into the magnitudes involved. Assume $m^* = m_e$ the free electron mass, and $E_c - E_f = (1/2)\ E_g$. At 295°K, kT is about .025 ev. Under the above assumptions the value of n becomes 4.1×10^{-29} cm^{-3}. The result is that one free electron will be found in each 2.4×10^{28} cm^3 of diamond. Recent density measurements yield 3.515 gm/cm^3 as typical of the density of diamond, and one may thereby find the mass of this huge diamond (34). It has a mass over 14 times the mass of the earth. The fact that no diamonds at room temperature have a resistance near the value which is indicated above is explained by imperfections and surface conduction. For example, lattice vacancies are predicted to exist in a crystal lattice at a temperature above 0°K from thermodynamic considerations (42).

A semiconductor is broadly defined as a material with a conductivity between that of a metal and that of an insulator. Semiconductors are described naively as having negative temperature coefficients of resistance, but a more complete examination shows that resistance may either increase or decrease with temperature in impure materials. The application of quantum statistics to a simple model containing impurities shows that beginning at a very low temperature, charge carriers associated with states within the "forbidden" gap are liberated in increasing numbers with increasing temperature. After the Fermi level sweeps through the impurity state level to an electron energy a few times kT less than the impurity energy, the impurities are unable to add further to the conduction process. The increase in lattice vibrations caused by the rise in temperature is responsible for an increase of resistance with temperature such as is common to metals. The thermal excitation of electrons across the energy gap,

as discussed above in connection with diamond, also increases with increasing temperature. These three processes give rise in general to three regions of different slope on a logarithmic plot of resistivity vs temperature for an impure semiconductor. The high and low temperature regions do have a negative coefficient, and the intermediate region has a positive coefficient.

Using the word intrinsic to imply a property of a pure material and extrinsic correspondingly for an impure or imperfect material, it is apparent that intrinsic diamond is an insulator. Intrinsic germanium at 300°K with a much smaller energy gap is a semiconductor in the above sense.

Recombination Processes and Defect States

From the discussion above it is apparent that the increase in conductivity of a material by the absorption of radiation will be more or less significant as the material is more or less conducting in the absence of radiation, i.e., depending upon its "dark conductivity." The conductivity of an insulator may be changed a large factor by radiation, whereas no change is observed in zinc doped germanium at room temperature. Crystal imperfections introduce electron states at otherwise forbidden energy values and give rise to the picturesque but inaccurate references to electron states in the forbidden gap. Such expressions refer to energies that are allowed but are not energetically near other such states. When such states become too dense, an "impurity band" is formed. The present discussion will not include that possibility.

The effect of the position within the energy gap of a defect state upon the process by which an excited electron returns to the ground state will be considered. This will lead to a distinction between a trap and

a recombination center. The following description is given particularly in reference to photoconductive processes, but the same distinctions are important in some others among which are luminescent phenomena.

Consider an electron to be excited from the valence band to the conduction band by photon absorption. If there are no states in the energy gap, the carriers each contribute to conduction until they pass out of the crystal. If they are replaced by the contacts at the opposite ends when they leave the crystal (ohmic contacts), the conduction continues until the electron and hole finally recombine. Recombination directly across the gap is an improbable event in actual crystals when compared to other recombination methods. The event would yield a recombination radiation photon. The capture cross section for the process in a slice kT wide near the band edges given by Rose (40) is

$$S = (1.1\times10^{-23}/d)\ (h\nu/h\nu_o)^2\ (300/T)^{5/2}\ cm^2 \qquad (2.6)$$

wherein $h\nu_o$ is 1 ev, T is the absolute temperature, $h\nu$ is the width of the forbidden gap, and d is the penetration depth of the exciting radiation. For the carrier densities usually found in diamond this recombination process is unimportant. Recombination radiation has been observed by using injection to obtain the required density of carriers (43).

Recombination can take place via defect states which are hereby defined as states arising from any crystalline imperfection. Suppose the electron is captured at a defect state. If the probability for excitation back to the conduction band is greater than the probability that a hole will combine with the electron-defect state combination,

the defect state is called a trap; otherwise it is called a recombination center. It is thus seen that the conduction process is not ended when electrons, or analogously holes, are trapped. It is only delayed for the time spent in traps. Further, since the recombination center returns the electron directly to the valence band it terminates the conduction process.

Rose points out that insulators have a more or less continuous distribution of defect states throughout the forbidden zone and that although the density at certain energies may be relatively large in comparison, the quasi-continuum of states must be incorporated in any complete treatment of insulators. The quasi-continuum of states is more prominent in evaporated and polycrystalline films than in single crystals. This tends to suggest that clustering of defects and the location of chemical impurities at a variety of crystalline defects may account for much of the quasi-continuum of states in the forbidden gap.

Considering a distribution of states as just indicated, Rose separates traps from recombination centers energetically with a demarcation level. For electrons, assuming one class of defects with a common capture cross section s_n, the electron demarcation level D_n is the energy at which the re-excitation to the conduction band of a captured electron is just as probable as the capture of a hole by the state following the capture of the electron. The discussion for holes is entirely analogous to that given for electrons so that one also has hole traps, hole recombination centers, and a hole demarcation level. The electron demarcation level is defined by the expression

$$\nu^*_n \exp[- |D_n, E_c| / kT] = pvs_p , \qquad (2.7)$$

$|D_n, E_c|$ is the positive energy difference of the indicated quantities, the left hand side of 2.7 is the rate of thermal excitation of an electron to the conduction band, and ν^* is related to the highest lattice vibration frequency. Rose (39) has shown that a close examination of the component factors of ν^* is not necessary since from detailed balance considerations,

$$\nu^*_n = N_c v s_n . \qquad (2.8)$$

At a given temperature the attempt to escape frequency, ν^*, for a particular center is directly proportional to the capture cross section for that center. N_c is the coefficient of the exponential given in equation 2.1 and v is assumed to be $(2kT/m)^{1/2}$. One finds the constant of proportionality to be

$$\nu^*/s_n = 8m^* (\pi/h^2)^{3/2} (kT)^2 . \qquad (2.9)$$

Let p_r be the density of recombination centers unoccupied by electrons and n_r the density which is occupied, and let s_n be the capture cross section of an unoccupied recombination center for a free electron and s_p the capture cross section of an occupied center for free holes. Under photoexcitation with $h\nu$ slightly larger than the forbidden energy gap and with a volume rate of generation f of free electrons and holes, a density of electrons n and holes p is created. Assume that n and p are small in comparison to n_r and p_r so that direct recombination is unlikely. Then equilibrium demands

$$n = f\tau_n = f / p_r v s_n , \qquad (2.10)$$

and

$$p = f\tau_p = f/\, n_r v s_p \,. \tag{2.11}$$

Also note that s_n is not in general equal to s_p. Equations 2.10 and 2.11 are valid if the carrier mean free path is larger than the diameter of the cross sectional disc (39). Combining the above result with equation 2.1 to eliminate n, the result is

$$|D_n, E_c| = |E_{fn}, E_c| + kT \ln(n_r/p_r). \tag{2.12}$$

By analogous argument

$$|D_p, E_v| = |E_{fp}, E_v| - kT \ln(n_r/p_r). \tag{2.13}$$

The demarcation levels are seen to be displaced equal amounts and in the same direction from their respective steady state Fermi levels. If another set of centers exists with its own s_n and s_p there will be another D_n and D_p for the second set which will be displaced in accordance with the above relations from the common steady state Fermi levels by the appropriate energies.

The rate of thermal exchange with the conduction band of states above D_n rapidly increases with displacement above D_n. For room temperature a displacement of .12 ev above D_n brings an increase of $e^{4.8} \approx 10^2$. These states return about 100 electrons to the conduction band for one which recombines with a captured hole. The states above D_n are seen to be in thermal contact with the conduction band, and their occupancy is given by a modified Fermi function centered on E_{fn}.

At this point, after a very brief treatment of recombination and trapping processes the subject will be concluded at what is really its

beginning because it would not add appreciably to the present study. Rose (40) points out the complex nature of photoconductive phenomena involving defect states with the statement, "The variety of dependencies of photocurrent on light and temperature is substantially unlimited. This statement is born out experimentally by the fact that photocurrents have been observed to increase linearly, supralinearly, and sublinearly with increasing light intensity. Similarly, photocurrents have been observed to be insensitive to temperature as well as increase or decrease with increasing temperature." Rose reduces the variety of behavior to six major patterns that need to be accounted for and proposes a model for each. No further discussion of them will be taken up in Chapter II. The reader is referred to his fine new book for details (39).

Photocurrent and Photoconductive Gain

Consider an insulating crystal of unit cross sectional area and length L between the anode and the cathode. The contacts are assumed to be broad ohmic contacts which are able to supply charge carriers as needed by the crystal. Let the crystal be uniformly irradiated such that a uniform absorption rate f exists throughout the crystal. For simplicity let radiation of energy $h\nu$ excite electrons from defect states to the conduction band in order to exclude hole conduction. If the lifetime of the free electron is τ the equilibrium number of photo-generated electrons is

$$N = F\tau \qquad (2.14)$$

where F is the total generation rate for the crystal. This result is independent of traps. Detailed balance requires that for each electron

trapped an electron must be liberated into the same state so the net effect is as if no trapping had occurred. If T is the transit time of a free electron from the cathode to the anode the photocurrent will be

$$I = Ne/T = eF\tau/T = eFG \qquad (2.15)$$

wherein the photoconductive gain G is the ratio of the electron current to the photon current. Thus, it is apparent that the concept of unit gain revered by early researchers is of no particular significance. One can continuously vary G by changing the electrode spacing and the applied potential. Only with special limiting contacts is unit gain meaningful. For example, the photocurrent in a photoelectric cell has unit gain. In the present case the transit time T is given by

$$T = L/v_d = L/\mu E = L^2/\mu V \qquad (2.16)$$

where v_d is the drift velocity, μ the electron mobility, and E is the electric field strength which is equal to the applied potential V divided by electrode separation L in the present case of ohmic contacts. Combining equations 2.15 and 2.16 yields

$$I = (eF\mu\tau/L^2)\ V \qquad (2.17)$$

First notice that the important parameter describing the photocurrent is the free carrier lifetime since the others are readily adjustable. Second, for voltage-independent μ and τ the I vs V relationship is linear. Provided no other effect intervened it is apparent that the photoconductive gain could be increased ad infinitum by adjusting V and L. Rose (39) points out that space charge limited currents intervene due to carrier injection at the cathode. By analogy with the

vacuum photoelectric effect and the Child-Langmuir relation he derives for the case of an ohmic contact on an insulator the approximate space charge limited current relation

$$I = (K \mu V^2 / 4\pi L^3) \times 10^{-12} \text{amp/cm}^2 \qquad (2.18)$$

K is the specific dielectric constant, the other symbols are as above. If shallow traps are present such that the ratio of free electrons n to trapped electrons n_t is small, and

$$\Theta = n/n_t \ll 1, \qquad (2.19)$$

then 2.18 may be written

$$I = (K \mu \Theta V^2 / 4\pi L^2) \times 10^{-12} \text{amps/cm}^2 \qquad (2.20)$$

Shallow traps increase the transit time of the injected carriers. The expression 2.18 will be evaluated for holes in diamond. Using K = 5.67 (44), μ = 1300 cm^2/volt sec. (12), V = 100 volts, and L = 6.5 cm, an upper limit may be established for the space charge current in DS-2 assuming an ohmic cathode. This is probably not a good assumption at low potentials. The above substitution yields

$$I = 1.6 \times 10^{-7} \text{ amps/cm}^2 \qquad (2.21)$$

For DS-2 the area = 7.5 mm^2 and

$$I = 1.2 \times 10^{-2} \mu a \qquad (2.22)$$

This value would be observed as "dark current" under the assumptions made above. The fact that dark currents measured at low temperature were less by a factor of about 10^3 would appear to indicate a barrier

at the electrical contacts to the diamond and possibly a large trapped carrier density.

Imperfection Photoconductivity in Semiconducting Diamond

The model necessary to describe diamond accurately includes more than one kind of imperfection. A simple model containing N_A monovalent acceptors and N_D monovalent donors such that $N_A > N_D$ will be used to discuss the p type conductivity exhibited in semiconducting diamond. An acceptor causes one state to appear at an energy above each band in the crystal (3). Thus three states are to be expected in the energy gap of diamond for each acceptor. Two states correspond to the bands which are doubly degenerate at $k = 0$ and the third one corresponds to the split off band which is 6×10^{-3}ev lower. Only one state is empty in the present model but since it can accept an electron in two spin orientations and is degenerate by a factor g=2 due to the band degeneracy, the probability of the acceptor state being occupied by a hole is given by the modified Fermi function applicable to diamond (45),

$$f_A = 1/(1 + 4\exp\left[(E_F - E_A)/kT\right]) \qquad (2.23)$$

Note that when the Fermi level E_F is at the acceptor energy E_A and $T > 0$ the states are 20 per cent occupied by holes.

At a sufficiently low temperature it is reasonable to take $n = n_D = 0$ where n and n_D respectively refer to the density of electrons in the conduction band and electrons bound to donors. For electrical neutrality the positive charge must equal the negative charge whereby one writes

$$p + p_A + N_D = N_A \qquad (2.24)$$

The notation corresponds to that of Shockley (3). The density of holes in the valence band is represented by p, the density of holes bound to acceptors is p_A, a monovalent donor is a singly charged positive ion, and a monovalent acceptor is a singly charged negative ion.

The greatest number of states which can bind holes is evidently given by (2.24) when p = 0 and is

$$p_A = (N_A - N_D). \tag{2.25}$$

The use of (2.23) gives p_A as a function of temperature and one has

$$p_A = N_A \cdot f_A \ . \tag{2.26}$$

The use of (2.26) in (2.24) provides the hole density p in terms of the remaining quantities

$$p = \{ N_A / (1 + (1/4)\exp[(E_A - E_F)/ kT]) \} - N_D \ . \tag{2.27}$$

The result (2.27) may be equated to the general equation for holes in the nondegenerate case to yield

$$\{ N_A / (1 + (1/4)\exp[(E_A - E_F)/ kT]) \} - N_D = N_V \exp[(E_V - E_F)/ kT]. \tag{2.28}$$

This result may be solved to yield a quadratic equation in $\exp[(E_V - E_F)/kT]$, and finally a complicated expression may be found for the Fermi energy as a function of the temperature, $(N_A - N_D)$, and N_V. The desired result may be derived more easily, however, from equation (2.27) for the case p = 0 corresponding to T = 0. Thus one is led to the limiting form

$$E_F = E_A - kT \ln[4(N_A / N_D - 1)], \qquad (2.29)$$

which shows that the Fermi level starts from the acceptor energy at T = 0. Blakemore (45) points out that this must always happen regardless of how small the fractional compensation since if there are any compensating impurities at all, the acceptors are partly ionized at T = 0. Note that the Fermi level shifts toward or away from the valence band edge with rising temperature depending on whether N_A is greater or less than 1.25 N_D. It was originally assumed that N_A is greater than N_D. Hall measurements indicate that N_A is greater than twice N_D. To find the temperature where E_F crosses E_A one may set the two values equal in (2.28) and find

$$\exp[(E_V - E_A)/ kT] = (.8N_A - N_D)/ (4.82 \times 10^{15} T^{3/2}) (m^*/m_o)^{3/2} . \qquad (2.30)$$

The numerical value for N_V is given by Shockley (3) and the correction for m* is indicated. The result given by Rauch for m* indicates that this correction will not be large, and it will presently be ignored, since at best the calculation (2.30) is approximate. Spin resonance studies indicate $(N_A - N_D) = 4 \times 10^{14}$, therefore the solution to (2.30) can be found (20). The value 0.22 ev found by Halperin and Nahum will be used to approximate the value $(E_A - E_V)$ whereby equation (2.30) becomes approximately

$$\exp 2550/T = 15 T^{3/2} . \qquad (2.31)$$

The equation was solved by a graphical method and the solution is 235°K. This result has special interest to the writer because it supports his earlier conclusion regarding the temperature dependence of phosphorescence in semiconducting diamond. At room temperature the

0.22 ev acceptors are ionized and the acceptors at the next higher activation energy are the traps which give rise to the observed phosphorescence. As the temperature is reduced the Fermi level shifts toward the 0.22 ev level and they give rise to a phosphorescence which is observed at reduced temperature (18).

The result calculated above has the following implication for photoconductivity. At liquid nitrogen and lower temperatures almost all of the uncompensated acceptor states contain bound holes, conduction is very feeble and photoexcitation should reveal the state nearest the valence band edge. Essentially no change is to be expected in the spectral response between 77° K and 4.2° K except that due to carrier scattering since the defect states are already essentially filled at 77° K. Since trapping should not exist, the steady state situation under generation rate f is

$$f = p\,(s_p\, v\, p) = p^2\,(s_p\, v)\,, \qquad (2.32)$$

The photocurrent is proportional to $f^{1/2}$ in this case if the Fermi level does not shift appreciably under irradiation.

The above discussion has ignored the extra activation energies reported by Halperin and Nahum, but they would only complicate the mathematical analysis and would not improve the discussion which is an approximation of the actual state of affairs.

Competing Mechanisms

The photosignal depends upon the fractional change $\Delta p/p$ in carrier density. At a low temperature, as discussed in the preceding paragraph, the dark current is small and even low levels of radiation can bring a significant fractional change in free carrier density. The free carrier

excitation rate may not equal the incident photon flux, however, since photons may be utilized by mechanisms which do not contribute to photoconductivity. The lattice absorption bands are a good example. Holes bound to acceptors may be raised to excited bound levels in keeping with the "hydrogen atom" approximation of a defect state. Transitions between bound states, luminescent processes, and intraband transitions can also compete for the available photons. Exact analysis is difficult and is further complicated by reflection at crystal surfaces and the uncertainty regarding the radiant path length within the crystal. Further consideration of this point is deferred to Chapter 4.

CHAPTER III

EXPERIMENTAL CONSIDERATIONS AND INSTRUMENTATION

Introduction

In the present chapter is a discussion of the instrumentation developed for the experimental work and some of the problems which were considered. The first subject to be treated is the photoconductive signal as it applies to the work. The optical problem is then discussed prior to the description of the electrical circuitry and the recording of data. Finally, a discussion of the development and use of the cryogenic equipment is given.

The Photoconductive Signal

General Discussion

It is advantageous to utilize chopped radiation techniques in photoconductive experiments on specimens which contain deep traps because of the very long decay times which cause large time delays for the establishment of equilibrium. This experimental technique will be referred to as an ac technique or ac photoconductivity. It should be remembered that the alternating signal is caused by the alternating intensity of the radiant flux incident on the specimen. The wave form and signal magnitude depend on the change in number of free carriers which can be established between the "on" and "off" portions of the chopping

cycle. In this regard one would like to have a very short decay time for waveform preservation in certain experiments such as detection of a cyclotron resonance signal using pulsed magnetic fields. The sensitivity of a photodetector is reduced as the free carrier life time is reduced. When one does not need to preserve a complex waveform a longer carrier life time up to a fraction of the chopping period is desirable.

The photoconductive signal will be derived for a simple model in which the specimen is in equilibrium with regard to the average number of carriers in traps, and the output signal is determined by the free carrier life time. This is not necessarily a good description of the real situation in many crystals including diamond but will serve the present need.

Photoconductivity resulting from excitation of carriers from states in the "forbidden" energy gap may be thought of as an internal photoelectric effect. After photoexcitation, an electron or hole is free to move in the periodic crystalline field and may be continuously accelerated to higher energy states. Finally the carrier is either recaptured, trapped, or swept out of the crystal at an electrical contact. The situation is different from intrinsic photoconductivity in which two carriers are created with each photoexcitation. In the simple model being considered, one has the governing differential equation for the increase in carrier density

$$\frac{d\,(n - n_o)}{dt} = g - \frac{(n - n_o)}{\tau} \tag{3.1}$$

where g is the rate of excitation within the crystal and τ is the free carrier life time. For an initial density n_o prior to the

incidence of the photon flux one finds

$$n = n_0 + g\tau\ (1 - \exp\ [-t/\tau]\ ), \qquad (3.2)$$

showing the equilibrium density to be

$$n = n_0 + g\tau. \qquad (3.3)$$

As previously discussed, traps do not change the ultimate value of n since it is the free carrier life time which determines it but traps cause a change in the response time of the photoconductor. Depending on the magnitude of the appropriate value of τ, equilibrium may never be reached in ac photoconductivity.

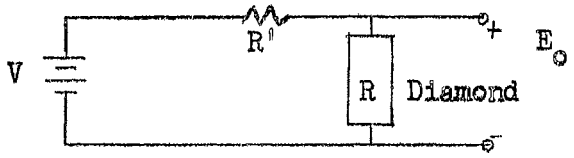

Fig. 1. The circuit used to discuss the photovoltage developed across the diamond. In practice R must be replaced by the complex impedance of the diamond in parallel with the input to the isolation amplifier, including the connecting cable.

The circuit considered is represented by Fig. 1. The output voltage is

$$E_0 = \{V/(R' + R)\} \cdot R = V/(1 + R'/R) \qquad (3.4)$$

where $R = L/(A\sigma) = L/(Aq\mu n)$, L and A are the length and cross section area of the crystal of carrier mobility μ, carrier density n and charge magnitude q. The conductivity of the crystal is $\sigma = nq\mu$. Assuming τ to be small with respect to the chopping period, one finds the following carrier density and ac signal output in a sine wave approximation

for the generation rate $g = g_o(1 + \sin \omega t)$.

$$n = n_o + g_o \tau (1 + \sin \omega t) \tag{3.5}$$

and

$$E_o = V \Big/ \left[1 + (R'A\, q\, \mu/L)(n_o + g_o \tau (1 + \sin \omega t))\right] \tag{3.6}$$

E_o may be increased by reducing n_o and increasing V and g_o. The dark conductivity may be reduced by cooling the crystal to prevent phonon excitation of carriers into conducting states and by the elimination of any background radiation of energy sufficient to excite carriers to conducting states. This is not to be confused with chopped scattered light from the monochromator which can directly produce a spurious ac signal and would appear as a part of g. It is of course apparent that if n_o is zero the crystal has infinite impedance during the half of the chopping cycle when the signal radiation is blocked. The dc resistance does become large in the diamond, but the impedance cannot exceed a value limited by the capacitance due to the electrical contacts. Contacts and impedance considerations are significant problems to be discussed.

Signal to Noise Ratio

The signal to noise ratio is the all important factor in the detection of any signal. The subject of noise has been treated by various authors, and a very useful discussion is given by Jones (46). The limiting noise in the present work is believed to be contact noise. The problem of making a mechanically strong contact to diamond can be approached in various ways. Grodzinski (47) discusses

various means of holding diamonds for grinding operations. Diamonds may be embedded in silver solder for example. For electrical contact one may use graphite, silver paint, and metal probes. Robertson, Fox, and Martin (4) used Wood's metal as a solder contact when the crystal was not subjected to a large temperature change during the experiment. The Wood's metal contact shears off the diamond if the assembly is placed in liquid nitrogen. Silver paint has been used by the author and by others (11, 21), however, it was felt that the organic binders used in the available silver paints made them unsuited for low temperature electrical contact to diamond in this work. A contact was made to diamond by soldering the cleaned and degreased crystal with indium metal. Indium will adhere to diamond if the clean crystal is heated by the molten metal. A sweeping action with a small soldering iron gave a broad contact which did not break loose from the crystal. The resistances of such contacts varied and the contacts were somewhat rectifying. The problem of making contacts was studied in the present work only to the extent that usable contacts were obtained. The dc bias voltage was always selected by finding an optimum signal to noise ratio. The bias voltage on one of the crystals used in this work in the low temperature scans was 225 volts. This is a typical value for all of the bias voltages. The dc crystal resistance was nearly 10^{11} ohms. The entire crystal was flooded with the input signal flux insofar as this was possible in order to fully utilize the signal radiation and prevent crystal polarization. It is believed that no photovoltaic effect was recorded in the work. In order to avoid surface currents which can contribute to the noise problem the crystal surface and all of the surfaces which might allow a leakage current were carefully cleaned.

Most of these surfaces were in vacuum so that moisture, a common trouble source, was eliminated from nearly all of the high impedance portions of the circuit. The relative humidity in the laboratory was generally between 35 and 45 per cent.

One noise source in the work was due to mechanical and acoustic vibrations. The cryogenic and electrical shielding were not perfectly rigid. It was not possible to use very large clamping forces on the cryogenic parts so the supporting table for the apparatus was mounted on Korfund Vibro-Isolators and weighted with 8 x 8 x 16 in^3 solid concrete blocks to provide a resonant oscillation frequency of about two cycles per second. This severely limited the low frequency vibrations. The high frequency vibrations which are transmitted through such a supporting assembly were removed from the signal by electrical filtering. The chopping frequencies used were 11 and 15 cycles per second, and twin-T filters tuned to these frequencies were used in the amplifying circuits. Since the radiation was always carefully focused so that the radiant image just covered the crystal, a relative shift between them would introduce a large noise signal. In the work with the IR-7 the mass of the instrument and its mount, and the method of suspension of the Nernst glower precluded any possible trouble from motion of the radiation beam. The vibration isolators prevented such motion of the diamond. For the experiments with the DK-1, the instrument was placed upon the "vibration-free" table with the diamond and no relative motion was possible. The crystal was supported by an angle iron frame placed upon a base of the previously described concrete blocks. Thin felt pads were cemented to the blocks to further reduce vibrations and to remove any tendency for slipping.

The elimination of 300°K background radiation is particularly vital when working with crystals such as copper or mercury doped germanium. They are sensitive to 10 μ radiation and therefore "see" the background as a noise source. In order to remove background radiation as a possible noise source, the diamond was surrounded by a shield made from aluminum foil. The copper mount was covered with aluminum foil so that the diamond was in a bright metal cavity which was at the temperature of the cryogenic fluid in use, i.e., either 77°K or 4.2°K. Thus any signal radiation which was not totally absorbed during passage through the crystal was reflected back onto the diamond. This technique provides a significant improvement in the signal to noise ratio.

Optical Considerations

The monochromators utilized in the work were integral parts of recording spectrophotometers so that the problem of a radiation source was already solved. The instruments used in the work were the Beckman IR-7 and the Beckman DK-1. They were modified electrically as will be discussed later. An optical system was designed for each instrument and they will be discussed separately.

The IR-7 System

The IR-7 is a double beam infrared spectrophotometer with a double monochromator. A purging attachment removes CO_2 and H_2O from the atmosphere within the instrument. An interchange system is used by which one may insert a grating and prism into the instrument for work within a given portion of the infrared spectral region. A sodium chloride prism is used in the near infrared region from 2 to 16 μ

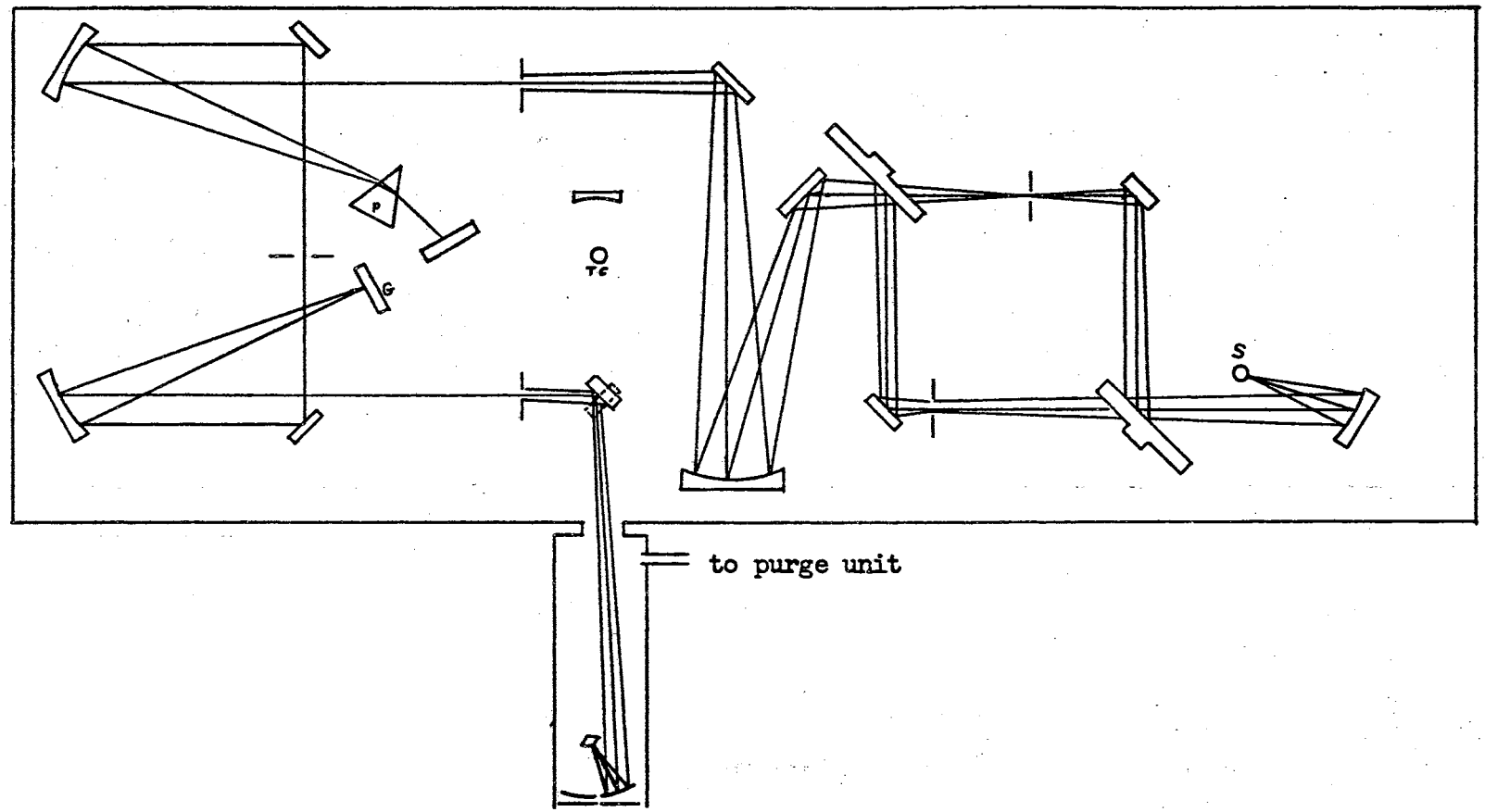

Fig. 2. The modified IR-7 optical path.

and a cesium iodide interchange is used in the 15 to 40 μ range. On each interchange a Littrow mirror behind the prism provides two dispersions of the radiation which is then passed through a central slit and thus enters a grating monochromator. The prism serves as an "order sorting" device for the grating which provides large dispersion. At 10 μ the dispersion shown in the Beckman manual is 1.8 cm^{-1} per mm slit width. The IR-7 uses a Nernst glower as its radiation source. A portion of the radiation falls on a phototube which provides a signal used to stabilize the dc power supplied to the glower. The instrument uses a special mirror for the long wave-length interchange. The spherical mirror which directs the source radiation into the instrument provides diffuse reflection for visible light and thus scatters the undesired high energy band when one wishes to work at wavelengths covered by the cesium iodide interchange. The sample compartment of the instrument is located between the source and the monochromator; at this position the instrument under consideration has two cesium iodide windows in the optical path. They are used to prevent the entrance of CO_2 and H_2O into the entire instrument when the sample compartment cover is raised in normal instrument use. The two windows cause a loss of not less than 30 per cent of the radiation from the source when they are in good condition, therefore they were removed for the present work. The optical path was further modified by supplying a rotatable mirror mount for the diagonal mirror which follows the exit slit of the monochromator. The rotation axis was in the reflecting front surface of the mirror. The beam was brought out through a window holder attachment which was installed on the monochromator cover. The instrument was operated in the single beam mode in the present work.

A concave mirror was mounted in the optical path such that an image of the exit slit could be formed with size equal to the face of the diamond to be irradiated. Adjusting screws provided a means of precisely aligning the mirror to obtain a maximum signal. The importance of the last step should not be underestimated. One can often gain a factor of 10 or more in the response due to fine adjustment of the mirror.

Upon removal of the two windows inside the IR-7, there was finally only one window in the optical system. This was the window on the vacuum cryostat which was necessary in order to admit the signal radiation to the diamond. The window materials used were NaCl and KCl. The percent transmission of these materials is almost constant in the spectral range covered in the work, and no correction to the data is required for a measurement of relative spectral response.

When working at invisible wavelengths, one must find a means of tracing the radiation through the optical path to allow component alignment and coarse adjustment. The use of mirrors avoids a chromatic problem including a shift with frequency in the focal lengths of certain elements. In order to bypass the dispersing elements in the monochromator, two mirror holders were devised such that a flat mirror could be placed in front of the prism and another in front of the grating. Upon adjusting them to pass the full spectrum through the central and exit slits, it was possible to focus a bright image of the slit upon the diamond.

The DK-1 System

In this section features which differ between the two systems will be discussed. The DK-1 is also a double beam instrument, but the sample

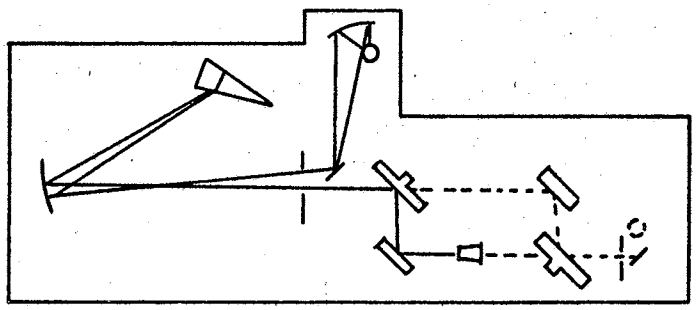

top view

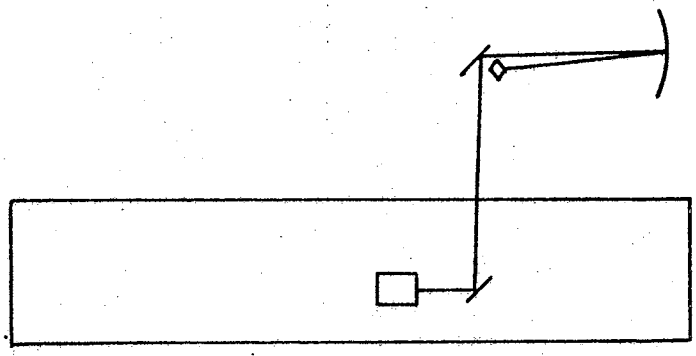

side view

Fig. 3. The DK 1 optical system showing the modification whereby the beam was brought out of the instrument and focused onto the diamond.

compartment, and consequently the chopping mirrors, follow the monochromator. This difference was of significance in the measurement of the radiant intensity versus wavelength and will be considered in a later section on radiant power determination. In the section on noise it was mentioned that the size of the DK-1 made it possible to mount the instrument directly upon the work table which had been suspended upon vibration isolators. In order to maintain the fine adjustment feature with the final concave imaging mirror it was found expedient to bring the beam out of the instrument. A simple device was constructed which attached to the DK-1 sample holder by a clamping action. This served to hold one diagonal mirror. A second diagonal mirror was sawed to a width such that when glued to an aluminum 45-45-90 triangular base the assembly could be placed in the sample holder just behind the cell holder. A felt pad was glued to the aluminum base to prevent sliding. By aligning the two mirrors the beam from the sample side of the instrument was brought up out of the instrument and then returned to its original direction. It was originally planned to utilize the reference channel and the instrument detection system to maintain the slit control in order to provide constant radiant power to the diamond. The electrical and optical modifications were made, but unfortunately the signal to noise ratio in the diamond photo-response was insufficient to record useful data because of the narrow slit settings provided in this mode of operation. The data were finally taken with constant slit settings. Fig. 4 shows the final mirror mounted as it was used. In front of it is the holder and the upper mirror used in bringing the beam out of the DK-1 reference channel.

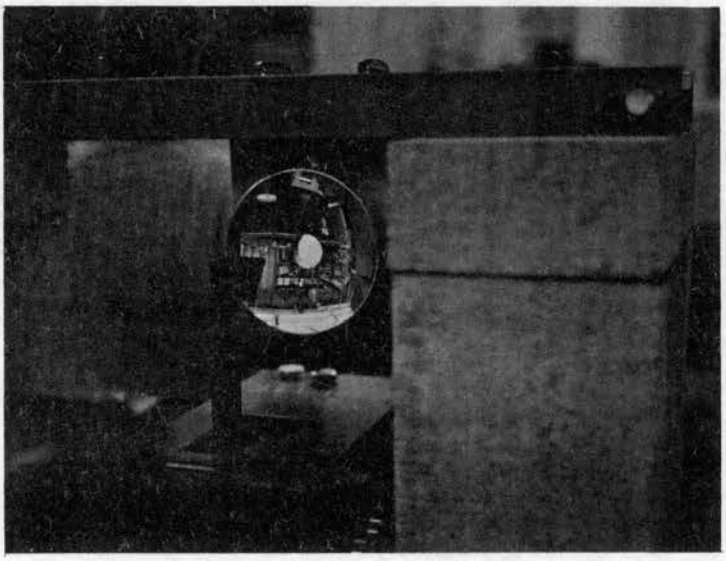

Fig. 4. The cryostat support and the mirror arrangement for the DK-1

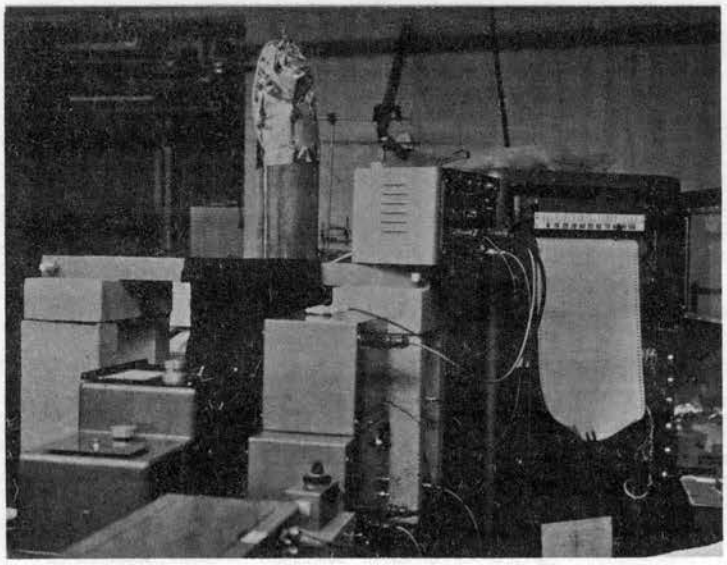

Fig. 5. The DK-1 system during a scan.

The Cryostat Support

The importance of stability was mentioned previously. In order to provide a sturdy vibration free support to the cryostat at a reasonable cost, two 8 x 8 x 16 in^3 solid concrete blocks with felt padded ends were placed on end and covered with a third block to form a support. An angle iron frame was placed across two such concrete supports. The angle irons were held together and spaced by 3/4 inch all thread bolts and nuts, one bolt and four nuts at each end. This support was quite inexpensive but was successful beyond expectation. Fig. 5 shows the mount in use during a scan.

Radiant Power Determination

To provide a means of reducing the data to give the relative photoconductive signal per incident photon, it was necessary to make a relative energy measurement of the flux incident upon the specimen. The energy measurement was made by placing a thermocouple at the position which was occupied by the diamond during the photoconductive experiments. The errors introduced by atmospheric absorption and contaminants on optical surfaces were largely cancelled. This method does not eliminate all the errors but was adopted because it appeared to offer the best determination of the incident flux which was in keeping with time and financial limitations which always exist in experimental work. The thermocouple, a Reeder model RBK-77S, was physically removed from the IR-7 but it was still electrically connected to the high voltage gain transformer in the instrument by means of a shielded extension cable. This allowed use of the Beckman low noise pre-amplifier and, for the IR-7 measurements, the rest of that instrument's electronics

and recording device. For measurement of the radiation from the IR-7 monochromator the beam was attenuated by the insertion of copper screens into the optical path within the sample compartment. The use of screen attenuators is preferred to excessive use of the trimmer comb because the latter can cause a false reading by preferentially irradiating a portion of the detecting element. Even thermocouples covered with gold black or other absorbers may be nonuniform in their sensitivity. In a recent personal communication with Charles Reeder, the writer was informed of research efforts with conical receivers which may ultimately eliminate the above problem.

The cesium iodide lens on the present thermocouple introduced what is believed to be only a slight error in the energy measurement. It was not possible to determine the percent transmission or polish the lens in the present case. The lens was only very slightly fogged and is considered to have achromatic transmission in the range in which it was used in the work.

A cylinder constructed of black paper joined the IR-7 to the final mirror, and an extra hose from the purging attachment was introduced into this enclosure to purge the optical path of CO_2 and H_2O. The purge was not sufficient, and the H_2O and CO_2 bands were recorded in these measurements. They introduce some uncertainty into the data but do serve to indicate the quality of resolution obtained in the work.

The measurement of the energy from the DK-1 monochromator was not as simple as for the IR-7. The instrument utilizes a 480 cps chopper and a 15 cps rotating mirror for beam alternation between the sample and reference channels. The thermocouple response to the 480 cycle component is negligible, and it served only to cause a net loss of

flux. As was mentioned earlier, the rotating mirror in the DK-1 follows the monochromator in the optical path and is located near the sample holder in the instrument. The thermocouple was precisely positioned at the place occupied by the diamond during photoconductive measurements. Unlike the IR-7 energy measurements, the thermocouple in the present case only "saw" the exit slit of the monochromator and its internal parts half of the time. During the "off" part of the mirror cycle the black wall of the mirror compartment housing was focused on the thermocouple. Thus, a 15 cps out-of-phase signal caused by 300°K background appeared in opposition to the desired signal. It is only through such experiences that one is really able to appreciate the sensitivity of some of the existing infrared detectors. Fortunately, it was possible to easily eliminate the 300°K background radiation by inserting a fused silica plate into the optical path. The thermocouple responds to practically all of the 300°K background, but less than 0.2% of such energy is transmitted by the fused silica plate. Using a special shutter the validity of this technique was verified, and the pen was found to read zero either when the DK-1 lamp was turned off or when the shutter in front of the thermocouple was closed.

The measurement was accomplished through interconnecting the IR-7 and the DK-1 with elements as shown in Fig. 14. It was not known that the 15 cps signal would pass through the filters in the IR-7 which is an 11 cps instrument. A strong enough signal was obtained to make satisfactory measurements. The signal from the White model 212A amplifier was sinusoidal so the discriminator circuit in the DK-1 was by-passed in the energy measurement. The input to the discriminator

was opened to prevent the introduction of an accidental signal. Due to the large value of R115 and the coupling mode used in the work, a slow pen response was encountered. Slow scans were necessary in order to obtain undistorted spectra. In both the IR-7 and the DK-1 energy measurements a graph was made for each slit setting which was used in the recording of data.

Scattered Light

An undesirable feature of grating monochromators is the transmission of scattered light. The monochromator in the IR-7 is designed in such a way that scattering is reduced significantly, and it is not a problem in the normal use of the instrument. In the present work the IR-7 served primarily as a source of monochromatic radiation. The amplifying circuits were generally adjusted to high levels. A particular effort went into the search for photoconductivity which should be observed in connection with the 0.2 ev activation energy recorded by Halperin (21), but the entire 2.5-40 μ range of the IR-7 was utilized in the study. Three photoconductive bands between 5 and 40 μ were recorded. One of them corresponded nicely with the above-mentioned activation energy. Since a fused silica plate in the optical path did not reduce the signal, it must be attributed to scattered light. The other bands were also found to be due to scattered light.

Electronic Considerations

The dark resistance of the diamond at low temperature is 10^{10} to 10^{11} ohms. It is therefore essential to have a high input impedance measuring circuit which does not electrically overload the diamond and lose the photo-signal. A dynamic cathode follower circuit

illustrated in Fig. 6 is based on a circuit designed by S. Zwerdling to whom this writer is indebted for a schematic diagram. For ac measurements it is capacitance which first limits the input impedance of ordinary circuits. The principle of operation of the present circuit is as follows. By shielding the signal lead from the ground lead and forcing the shield always to have the same potential as the signal lead, it is possible in principle to remove all input capacitance so that no charging current need be provided by the high impedance signal source. In practice there is always some capacitance even though the shield is taken as close to the detector as possible. For example, a load resistor switch was found to cause a shunt capacitance of several picofarads even after it had been redesigned and shielded. It was finally removed from the circuit.

A brief analysis of the circuit will be given. We will make use of Millman's theorem given by Seeley (48) which is applied to the general circuit shown in Fig. 7. The output potential difference is

$$E = E_1 Y_1 + E_2 Y_2 + \ldots / Y_1 + Y_2 + \ldots \qquad (3.7)$$

$Y = 1/Z$ is the admittance of the branch. The result is derived as follows. $I_1 + I_2 + \ldots = 0$ since the output is open. Therefore $(E - E_1)Y_1 + (E - E_2)Y_2 + \ldots = 0$. This may easily be solved for the above useful form. The potential sources E_1, E_2, etc., may represent real or fictitious sources. In order to simplify the overall treatment first consider the mid-frequency circuit shown in Fig. 8a and an equivalent shown in Fig. 8b.

Note from Fig. 8a that $Ei = Eo + Eg_1$, where Eg_1 is the ac voltage between the grid and cathode of the input tube which has dynamic plate

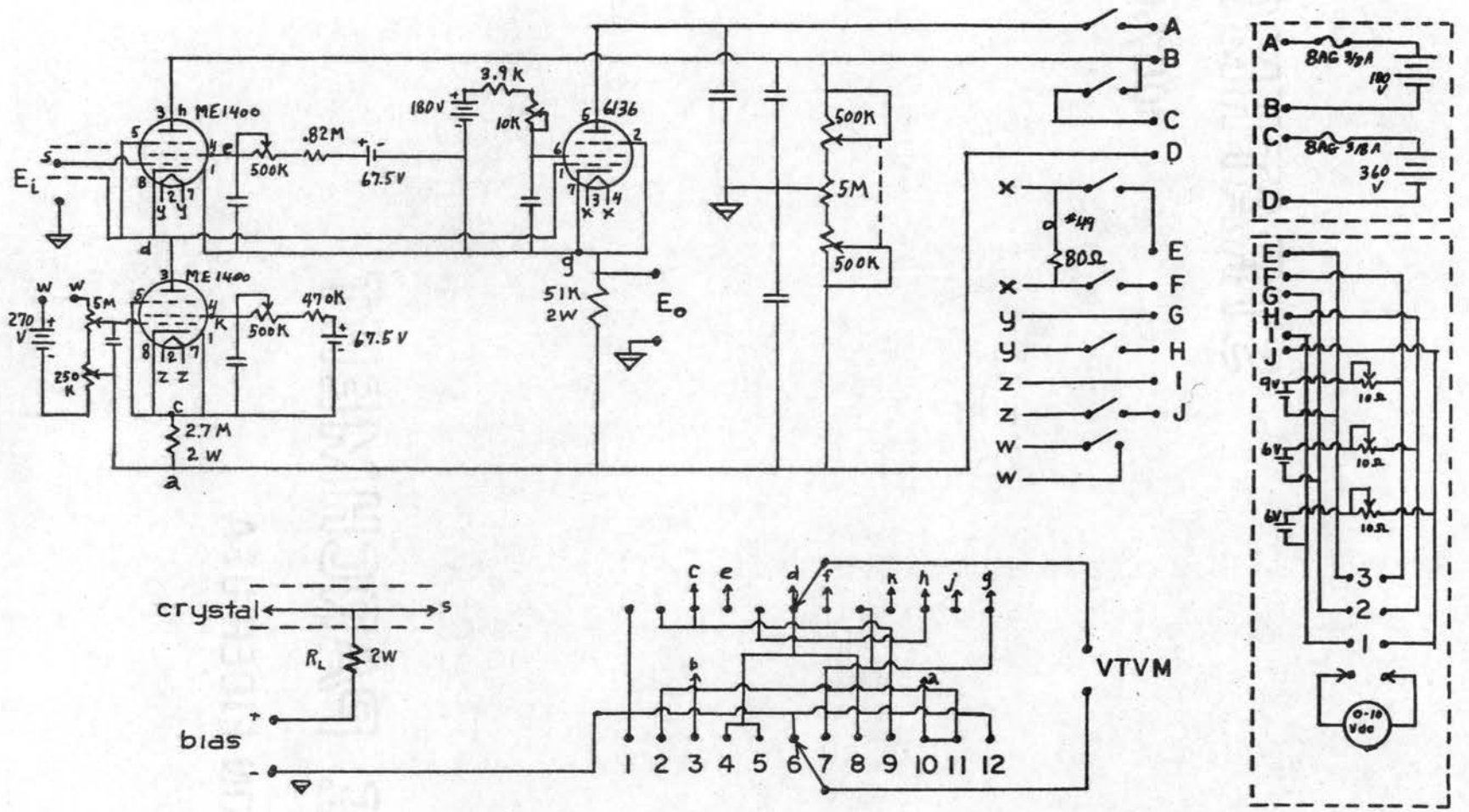

Fig. 6. The isolation amplifier circuit.

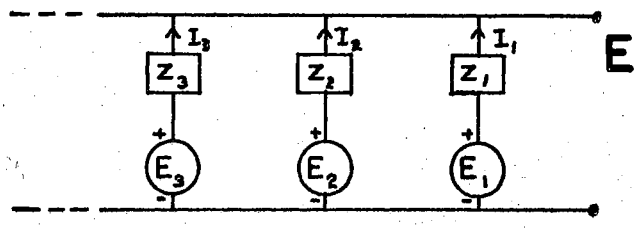

Fig. 7. Array used in the derivation of the Millman theorem.

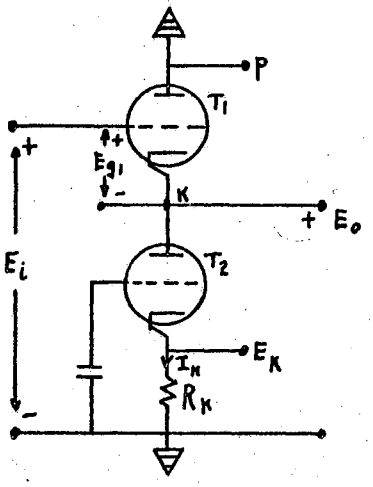

Fig. 8a. The ac representation of the input section of the isolation amplifier circuit for moderate frequencies

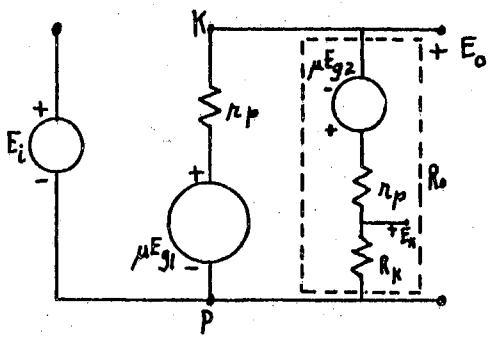

Fig. 8b. An equivalent circuit. The right hand branch may be replaced with a dynamic resistance R_o.

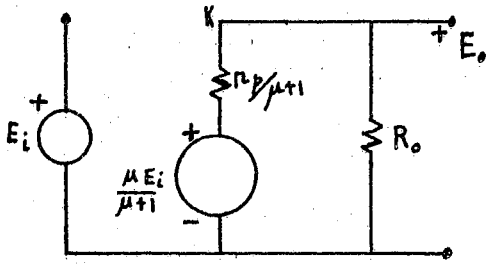

Fig. 9. Mid-frequency representation of Fig. 8a.

resistance r_p. This leads to the relation $Eg_1 = Ei-Eo$. Note further that $Eg_2 = -E_K = - I_k R_K$. The right hand branch in Fig. 8b yields

$$Eo = I_K(R_K + r_p) - \mu Eg_2 = I_K(R_K + r_p + \mu R_K), \qquad (3.8)$$

by substitution for Eg_2. We have the result that the right hand branch may be replaced with a dynamic resistance

$$R_o = (r_p + (1 + \mu)R_K). \qquad (3.9)$$

Using R_o to denote the right hand branch of Fig. 8b and using the Millman theorem we have

$$E_o = \mu(E_c-Eg_1)/\left[r_p /(1/r_p + 1/R_L)\right] = E_i \left[\mu/(\mu+1)\right] R_L/\left[(r_p/(\mu+1))+R_2\right]. \qquad (3.10)$$

This leads directly to the equivalent circuit of Fig. 9 and a gain for the feed back circuit of

$$KG = E_o/E_i = \left[\mu/(\mu + 1)\right] R_o/\left[(r_p/(\mu + 1))+R_o\right]. \qquad (3.11)$$

When one compares this with the gain for an ordinary cathode follower, the equations look the same, but the size of R_o is significant. R_K is effectively increased by a factor of μ which can be large. If μ is 10^3 we have $K \doteq 1$. The usual low output impedance $r_p/(\mu + 1)$ is obtained in this circuit and in this naive picture the input impedance is infinite since no input current was in the equivalent circuit.

Now add the following features. First, place a shield around the grid input and drive the shield from point K. Also, stray capacitance appears between the various elements of the circuit. Fig. 10a represents the real situation. The notation is as follows. Numbers 1 and 2 refer

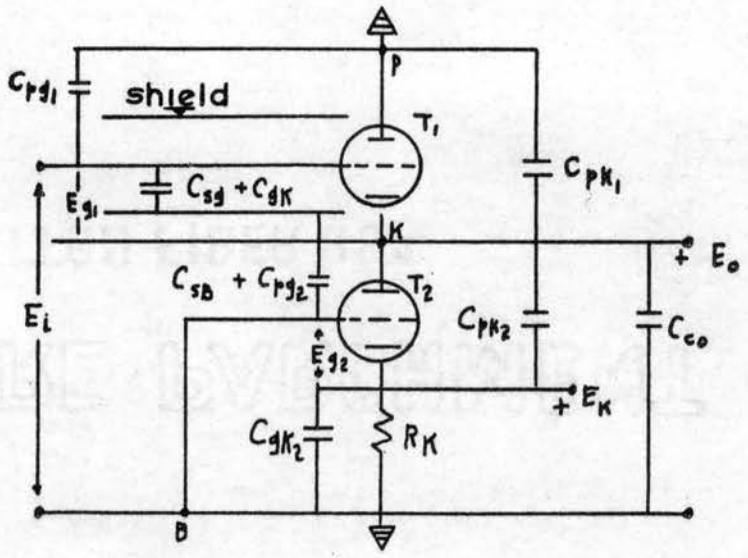

Fig. 10a. The high frequency ac circuit including the input shield.

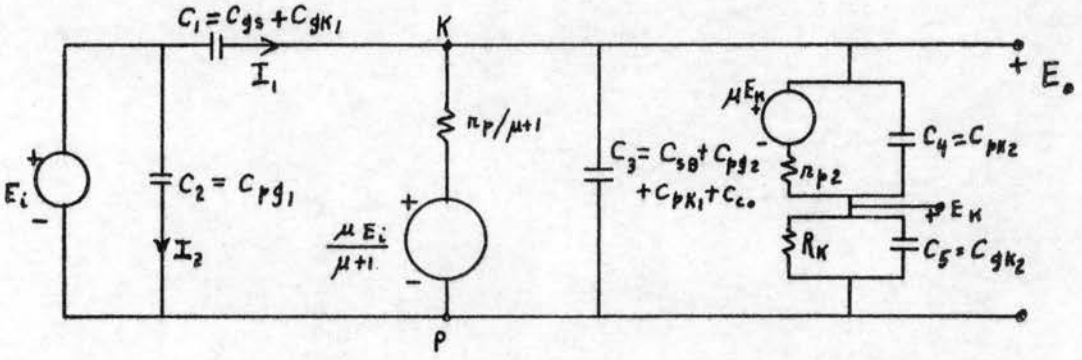

Fig. 10b. An equivalent circuit.

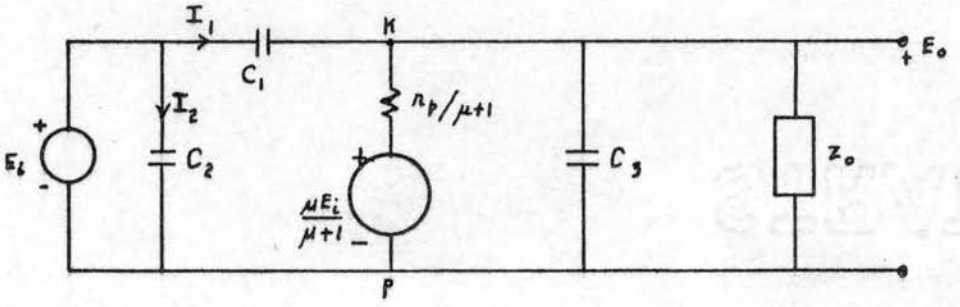

Fig. 11. Final equivalent circuit replacing the right hand branch with a dynamic output impedance Z_o, the analytical form of which is given in the text.

to the respective tubes; Cpg is the capacitance between the plate and grid with analogous usage of k for cathode and s for shield. Stray capacitance between the output and the next stage is given by Cco. Note that $E_{g_1} = E_i - E_o$ and $E_{g_2} = -E_k$. An equivalent circuit is given in Fig. 10b wherein $-E_k$ has been substituted for E_{g_2} with the appropriate change of polarity. The branch between K and P is the same as in the previous treatment, but the right hand branch is more complicated. One may use Thevenin's theorem on the portion between E_o and E_k. The open circuit voltage is found by use of the Millman theorem.

$$E_o - E_k = V_{Th.} = (\mu E_k/r_p)/\left[(1/r_p) + j\omega C_4\right] = \mu E_k/(1 + j\omega C_4 r_p) \tag{3.12}$$

where $r_{p_1} = r_{p_2} = r_p$. The Thevenin impedance is given by

$$Z_{Th.} = (r_p/j\omega C_4)/\left[r_p + (1/j\omega C_4)\right] = r_p/(1 + j\omega C_4\, r_p). \tag{3.13}$$

The branch between E_k and ground may be noted Z_k and is

$$Z_k = R_k/(1 + j\omega C_5\, R_k) \tag{3.14}$$

$E_k = I_k\, Z_k$ leads to a passive element representation of the Thevenin generator as in the previous treatment. Substitution for E_k yields

$$E_o - E_k = V_{Th.} = \left[\mu\, Z_k/(1 + j\,\omega C_4\, r_p)\right] I_k \tag{3.15}$$

Effectively, a two element complex impedance represents the right hand branch. The term $Z_1 = r_p/(1 + j\omega C_4\, r_p)$ and an impedance $Z_2 = \left[1 + \mu/(1 + j\omega C_4\, r_p)\right] Z_k$. Let $Z_o = Z_1 + Z_2$. It does not lead to a simplification to include C_3 in the branch.

The final equivalent circuit is given in Fig. 11. Using the Millman theorem one obtains

$$\left(\left(E_i\ j\omega C_1 + \left[\mu\ E_i/(\mu+1)\right]\ (\mu+1)/r_p\right)\right) \Big/ \left[j\omega C_1 + (\mu+1)/r_p + j\omega C_3 + 1/Z\right] \tag{3.16}$$

This leads directly to the following gain expression

$$E_o/E_1\ (gm + j\omega C_1)/\left[\left[gm + j\omega(C_1 + C_2) + 1/\left\{(r_p/(1+j\omega C_4\ r_p)\right] + \left[R_k/(1 + j\omega C_5\ R_k)\right]\ \left[1 + \mu/(1 + j\omega C_4\ r_p)\right]\right\}\right]\right] \tag{3.17}$$

Further reduction of the K_f equation did not add to its usefulness. By evaluation with the circuit perimeters the expression was found to remain complex at all frequencies. The real component is always much larger than the reactive component. The gain becomes a negative real number with a small inductive imaginary component at a few hundred cycles per second.

The input impedance is the most important feature of the amplifier. One obtains from Fig. 11, $I_{in} = I_1 + I_2 = (E_1 - E_o)\ j\omega C_1 + E_1\ j\omega C_1 + E_1\ j\omega C_2$ and since $E_o = K_f\ E_1$, $I_{in} = E_1 j\omega\ \left[(1-K_f)C_1 + C_2\right]$. The capacity C_1 is effectively reduced by $(1-K_f)$ but C_2 is not reduced due to cathode follower action. For this reason in such circuits one may use pentodes so that the plate to grid capacity can be kept extremely low. In the Mullard ME1400 tubes used in the present circuit this value is 20×10^{-15} fd. An alternative is to use a triode and drive the plate as did MacDonald (49). He used the ideas developed above to drive the plate of a triode input stage and achieved a low input capacity. In the present work the capacitance was limited by other factors and the

MacDonald Circuit was not needed; however, MacDonald's input impedance values do not appear to be as large as the values obtained in the present work. A General Radio Company model 716-C bridge circuit was used to obtain the input impedance values shown in Table II.

TABLE II.

FREQUENCY DEPENDENCE OF Z_{in} FOR THE ISOLATION AMPLIFIER

Frequency (cps)	Input Capacitance (pico fd)	Input Resistance (ohms)
100	.1	3.67×10^{11}
200	.15	2.3×10^{10}
500	.1	7.7×10^{9}
1000	.1	1.05×10^{10}
2000	.15	3.3×10^{9}
5000	.15	1.96×10^{9}
10k	.15	1.47×10^{8}
20k	.15	2.5×10^{7}
50k	.1	4.9×10^{6}
100k	-.05	$.93 \times 10^{6}$

Signal Amplification and Recording

The isolation amplifier discussed in the previous section was followed by a low noise high gain preamplifier in order to optimize the signal to noise ratio. A battery powered Tektronix 122A preamplifier which had been modified to further reduce noise was used for this purpose. The output noise level was not over 4 millivolts with the input shorted and gain of 10^3. This was far below the noise in the signal.

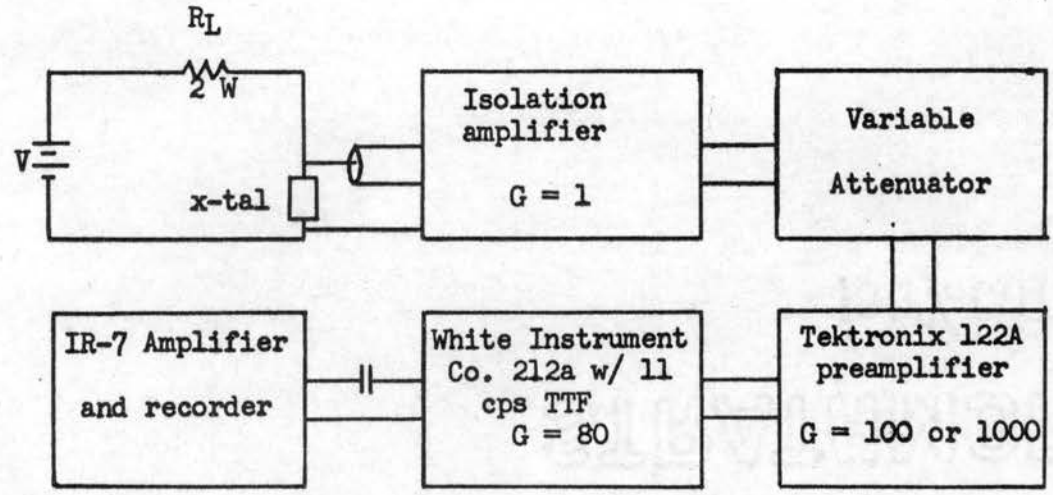

Fig. 12. Electrical apparatus for the IR-7 system.

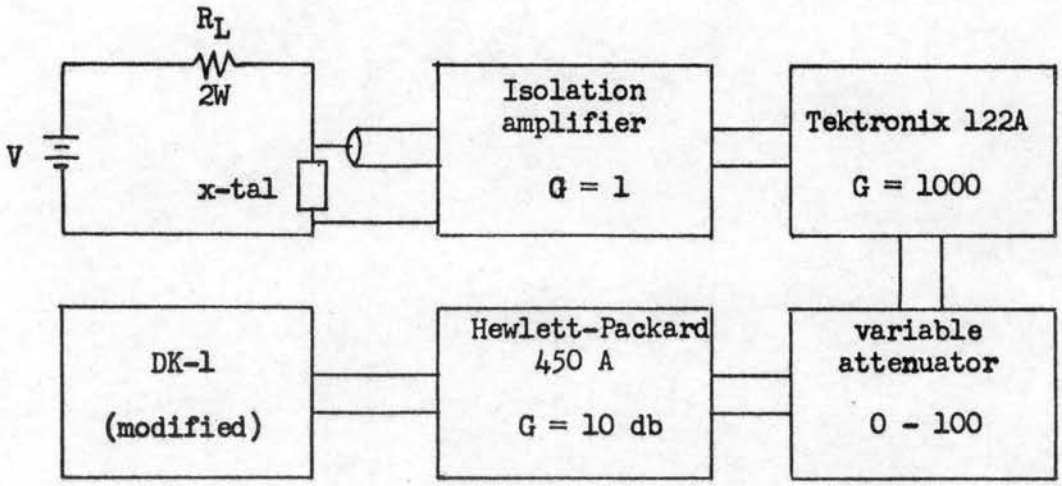

Fig. 13. Electrical apparatus for the DK-1 system.

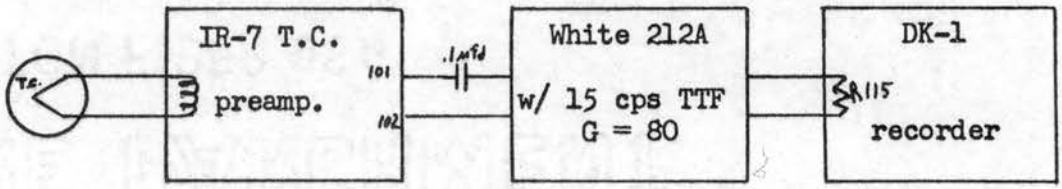

Fig. 14. Electrical apparatus for the thermocouple measurements of the radiant power which fell on the diamond.

In order to remove electrical pickup and signal due to acoustic vibrations and other undesired components in the signal, a White Instruments Company Model 212A amplifier with band broadening provision was used with a White twin-T filter, 11 cps for the IR-7 and 15 cps for the DK-1 during determination of the radiant energy with the thermocouple. The IR-7 was quite phase sensitive, and it was necessary to rephase the rotating mirror to optimize the response when the instrument was used.

The DK-1 is doubly filtered. This is because a 480 cps chopper is used in the instrument, and the rotating mirrors only serve as a beam splitter. The photovoltage is similar to a radio signal wherein a low frequency envelope appears on a high frequency carrier. The DK-1 uses a 480 cps detecting circuit followed by a discriminator which is finally followed by a 15 cps twin-T filter. There was no need to use additional filtering so the circuit of Fig. 13 was used for this part of the work.

The Cryogenic Equipment

General Remarks

The problems associated with work at liquid helium temperature are significantly greater than those one faces in work at liquid nitrogen or higher temperatures. This is largely due to the small latent heat of vaporization of helium. The helium atom has no tendency to unite with either another helium atom or an atom of one of the other elements. The lack of a tendency to form compounds or helium molecules is responsible for the fact that helium is a very poor refrigerant. The latent heat of vaporization is 0.62 calories/

cm^3 for helium, 58.1 calories/cm^3 for oxygen, and solid carbon dioxide sublines with the latent heat of 223 calories/cm^3. (51) The inertness of helium however is responsible for its usefullness as a low temperature refrigerant. The boiling point of helium at standard atmospheric pressure is near 4.2 degrees Kelvin.

The cryogenic equipment utilized in this work was developed by the author. The associated problems and their solutions were found to be interesting and will be discussed. Two books which have been most useful and are recommended to anyone planning work at low temperatures are Cryogenic Engineering by R. B. Scott (50) and Experimental Techniques in Low Temperature Physics by G. K. White (51). Various cryostat designs can be found in the literature. The one used in the present work is illustrated in Fig. 15 and was motivated by a paper published by Schoen and Broida (52). The "cold finger" design of these authors was adopted in order to minimize the off axis angle of the optical path. The arrangement for the radiation shield was found to greatly simplify the construction of the dewar; however, the design introduced a sensitivity to acoustic noise and vibrations into the electrical system due to the high impedance of the circuitry. This problem was partially solved by lightly clamping the metal parts to prevent their relative motion. The screws were made conical to the end to increase thermal resistance, and some utilized teflon sheets between the screw tip and the second surface to degrade the thermal contact. The dewar was at first used with a dynamic vacuum system, but because of the noise problem a static vacuum arrangement was devised and adopted. The Hoke valve permitted pump down prior to use of the dewar and is arranged so that valve closure does not

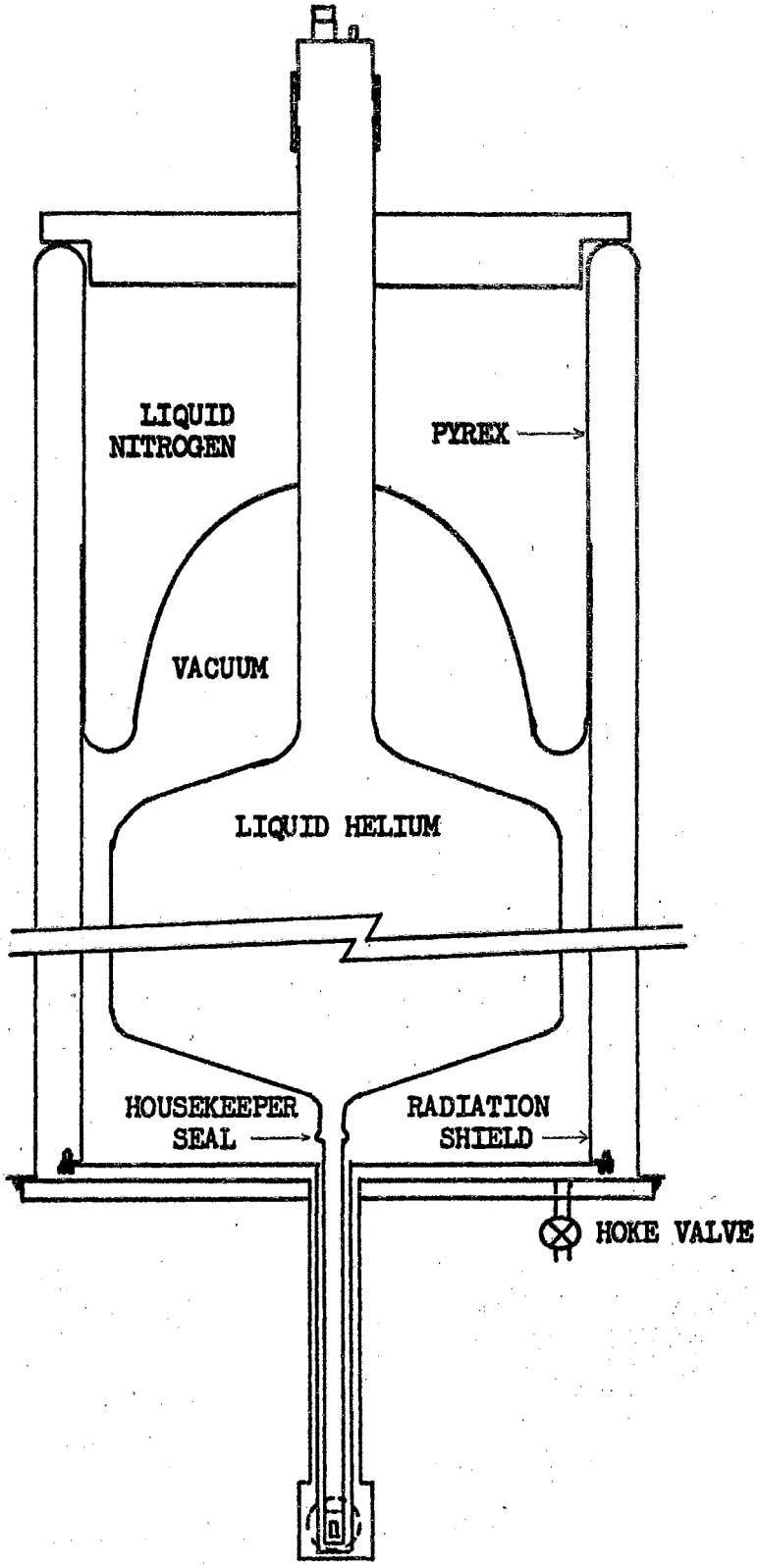

Fig. 15. The vacuum cryostat.

introduce a new "unpumped" surface which can spoil the vacuum. Several temperature measurements were made at the extreme end of the liquid nitrogen radiation shield. The temperature neared equilibrium at about 85°K in approximately 90 minutes and was sufficiently low for economical operation within thirty minutes. The shield was constructed of copper and was bright nickel plated because of the low tarnishing rate of nickel. Because of the small heat of vaporization of helium which was previously mentioned, it is essential that the container be precooled and that great care be taken to prevent any heat leak into the helium compartment. A calculation shows that if one kilogram (2.2 lbs.) of copper at ordinary temperatures were tossed into a lake of liquid helium, over three hundred dollars worth of liquid helium would be evaporated in the process of cooling the copper to 4.2° Kelvin. This estimate is based upon only ten dollar per liter cost for liquid helium. If the temperature of the copper is first reduced from 300 degrees to 90 degrees Kelvin by some other means, then the cost of cooling the copper to liquid helium temperature is approximately thirty dollars. An additional ten degree change in pre-cooling reduces the cost to approximately 24 dollars. This shows the importance of a few degrees in the pre-cooling process.

The technique used in the present work was as follows: Liquid nitrogen was placed in the outer jacket in order to trap remaining gas in the vacuum space. After several minutes delay, a quantity of liquid nitrogen was placed in the helium compartment and allowed to remain there for several minutes until the compartment was at the temperature of liquid nitrogen. With the special cap illustrated in the Fig. 15 it was possible to insert helium gas at the top of the neck of the

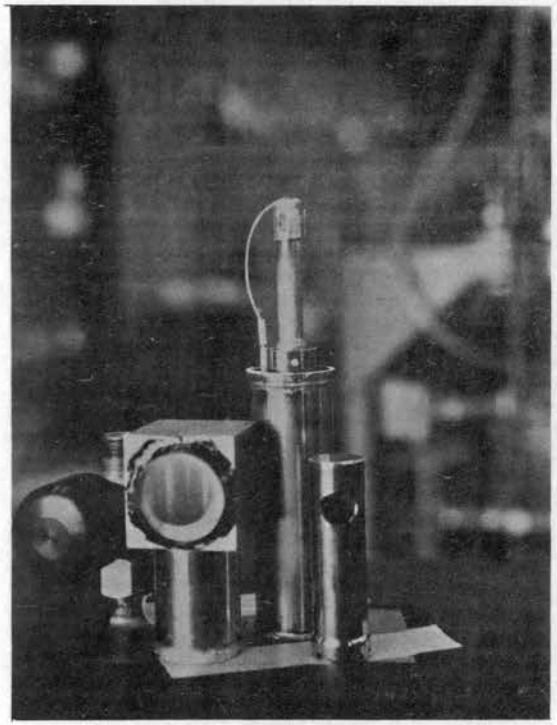

Fig. 16. Photograph of the "cold-finger" components. Woods metal was used to seal the outer tube.

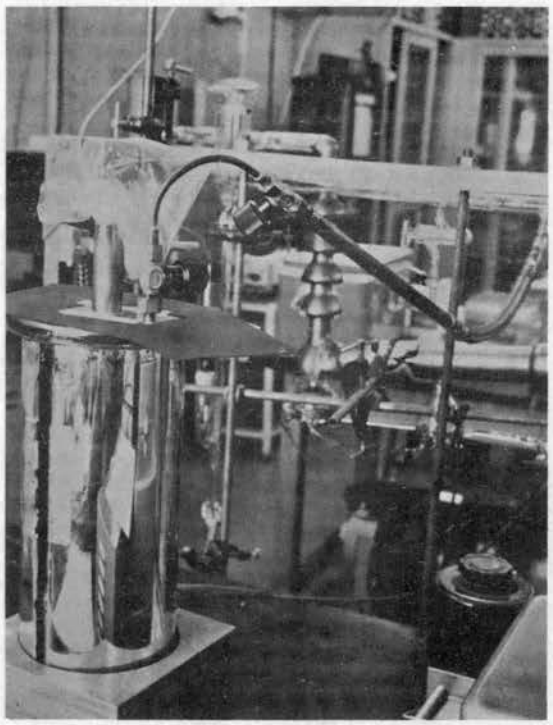

Fig. 17. The assembled cryostat being evacuated.

helium compartment and force the liquid nitrogen out through a 1/16" diameter stainless steel tube inserted to the bottom of the "cold finger." In this way the liquid helium chamber was rapidly pre-cooled and made ready for use. The amount of heat introduced with the warm helium gas was of no consequence. The technique not only permits rapid pre-cooling, but at the same time prevents introduction of air or water into the liquid helium compartment and proved to be quite satisfactory.

Heat Influx

The problem of heat influx involved the introduction of heat through radiation, conduction down the neck of the cryostat, and that which flows in through either electrical leads or thermocouple leads. Joule heating in the crystal must also be considered. Calculations were made involving each of the heat leaks and the results of these calculations will be mentioned.

The calculated power input to the helium by conduction down the glass neck from the 77° thermal source is 46 milliwatts. The power input from radiation to the walls of the liquid helium compartment is about 0.8 milliwatts. Although the mean value of the thermal conducitivity of copper is over 50 times that of the austenitic stainless steels such as the 304 alloy used in cryogenic work, the heat flow through two 36-gauge copper wires of 20 cm length is only 1.1 milliwatt. Since copper is easier to solder than either stainless steel or manganin, which was used at times during early phases of the experimentation, all of the data in this work were obtained using 40-gauge copper leads. The heat input due to the infrared and visible

radiation is ignorably small and the Joule heating in the diamond due to the dc biasing current is insignificant. It can be seen that the heat flux down the neck of the dewar is the dominant heat source in the present dewar. This can be reduced by a factor of four or five by using thin wall stainless steel tubing, but the fabrication of a stainless steel dewar is not readily accomplished with university facilities. The glass dewar was built by Wayne Adkins of the Chemistry Department glass shop. A feature of the dewar not originally adopted is that of strip silvering so that one can look inside the liquid helium compartment. There is no question that the small loss caused by 300° radiation influx is insignificant when compared to the accidental loss easily incurred when the liquid level is not known. The author made a liquid level finder of zinc coped germanium and successfully used it in some early work, but the stip silvered dewar offers greater advantages which are not at first obvious.

Specimen Mounting

The ease of mounting the specimen is important. Not only can time be wasted but equipment can be broken when it is difficult to use. The final design is by no means the original. The specimen mount used in the dewar allowed removal of the "cold finger" tube so that it is possible to solder a specimen to the mount and subsequently attach the mount to the dewar. The specimen is separated from the liquid helium by a .050" thickness of copper plus the thickness of the solder between the copper mount and the specimen. The proximity of the specimen to the liquid helium and the thermal conductivities involved are such that the specimen may be taken to be the temperature of the liquid in the dewar to the degree of exactness required in this work. The major uncertainties

are the thermal resistance of the boundaries between the specimen and the indium solder and the boundary between the indium solder and the copper. These uncertainties exist in thermocouple measurements wherein errors can also arise from thermal conduction through the thermocouple wires from the outside and between the junctions. The most suitable thermocouple material for the liquid helium range appears to be the gold doped with 2.1 atomic% cobalt versus copper. The NBS calibration data (50) for the material were plotted and used for some early work by the present author. In the liquid helium temperature range, the thermal emf of the above thermocouple is 3 to 4 microvolts per degree and the reference junction should be at helium temperature to avoid the effect of inhomogeneities. The error in the "assumed" specimen temperature is not likely to be larger than that which would occur if the temperature had been measured in the present experiment since the heat flow to the diamond was so small.

There are two aspects of the 300°K background radiation which strikes a photoconductor. One is the thermal influx. The other, which can be significantly more important, is the signal noise created by this radiation. In order to obtain the best signal to noise ratio in photoconductors which are sensitive to the 300° background, it is necessary to have a cold wall around the photoconducting specimen and have as small solid angle of "view" as is possible without restricting the signal radiation. In any case, the field of view should be restricted so that the photo-detector can only "see" the final mirror in the optical system if this is possible.

Electrical isolation was critical in the work due to the large impedance of the diamond at low temperature. The typical problem with

moisture on the surface was not experienced because the specimen was in vacuum. The teflon header used to hold the outer contact screw appeared to be adequate in the work; however, it would not be difficult to increase the length of the teflon path between ends of the diamond. The electrical leads were enclosed in teflon tubing so that the lowest resistance shunting the diamond was at the vacuum feed-through terminal which was epoxied onto the dewar. Since this terminal arrangement had been degreased, and since the relative humidity was generally less than 45% in the laboratory, it is believed that surface leakage currents contributed negligibly to the noise in the signal.

The Liquid Helium Transfer Tube

A liquid helium transfer tube was designed and constructed. The pressurizing tap was constructed with an o-ring closure rather than the usual rigid solder connection. This allows the transfer tube to be raised and lowered with respect to the storage and experimental dewars. The method for filling the experimental dewar consists in positioning the storage dewar at a predetermined height and distance from the experimental dewar by means of a hydraulic lift cart and then sliding the transfer tube down into the dewars to a predetermined level. The level is calculated to prevent all of the liquid helium from being transferred from the storage dewar. In unusual circumstances confusion regarding the quantity which has been transferred can arise. This precaution can prevent a significant loss in such cases. The sliding pressure tap also permits convenient pre-cooling of the transfer tube when one wishes to add liquid helium during operation.

The design of the tube is illustrated in Fig. 18. In addition to the sliding pressurizing manifold, another feature incorporated is the continuity of the inner tube. It was felt that the number of solder connections which are to be cooled should be minimized. If the tube has a vacuum leak one has only to look on the outside. Calculations showed that no bellows were necessary to allow for contraction. The inner tube was positioned toward the outer radius of the 90° elbows and isolation was verified with an ohmmeter prior to making the solder connections which determined the lengths of the outer wall sections. The teflon spacers were cut following Scott's suggestion. Soft soldering of the stainless steel tubing was easily accomplished with the aid of the Lake Chemical Company N-3 flux. This transfer tube has been entirely satisfactory.

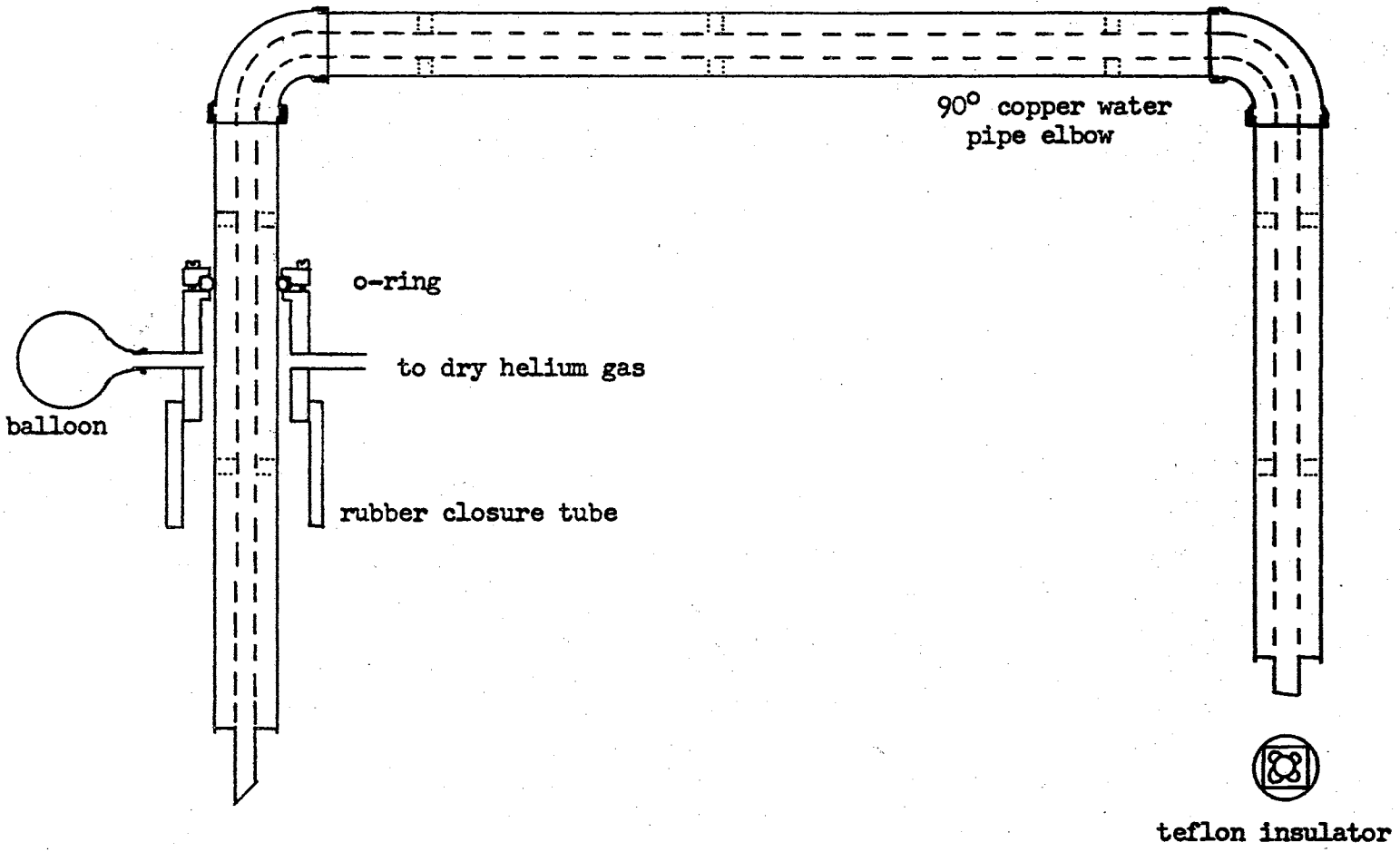

Fig. 18. Liquid helium transfer tube designed to provide a continuous inside tube. All solder joints are external.

CHAPTER IV

PRESENTATION OF THE DATA AND DISCUSSION

Preliminary Remarks

The present chapter begins with a discussion of the method by which the experimental data were reduced and then presents the reduced data in graphical form. The data are compared with data obtained by other means and in other investigations. From this comparison, certain conclusions are drawn and, finally, some suggestions are made regarding the direction of further studies.

Method of Data Reduction

When the effective carrier lifetime is small with respect to the period of the radiation cycle in ac photoconductivity, the steady state excess number of photo-excited holes, $(P - P_o)$, for semiconducting diamond is given by

$$(P - P_o) = G \tau \qquad (4.1)$$

during the time the crystal is being irradiated. Here P represents the number of holes during photo-excitation, P_o gives the number of holes in the dark, the total excitation rate is G, and the free carrier lifetime is τ. Let the excitation efficiency be represented by α. The total excitation rate is given by

$$G = \alpha N, \qquad (4.2)$$

where N is the number of photons per second which are incident upon the sample. This definition of α must include the possibility of reflection losses and other competing mechanisms, and it is assumed that the crystal is uniformly irradiated. The photocurrent is given by

$$I = (P - P_o)e/T_r \ , \tag{4.3}$$

where e is the electron charge and T_r is the transit time. The photocurrent divided by the photon incidence rate is proportional to the photo-excitation per incident photon and is given by

$$I/N = \alpha \ e \ \tau/T_r \ . \tag{4.4}$$

It can be seen from Fig. 1 that the output signal voltage is the photocurrent, I, multiplied by the load resistance, and the response curves $f(\nu')$ are therefore proportional to the photocurrent.

$$I = A \ f(\nu'), \tag{4.5}$$

where A is a linear amplification factor and $\nu' = 1/\lambda$. The power incident upon the specimen, $P(\nu')$, was measured by a thermocouple as previously described, and the curve $P(\nu')$ is related to the photon flux by

$$P(\nu') = N \ hc \ \nu', \tag{4.6}$$

where N represents the number of photons per second of energy $hc\,\nu'$ incident upon the sample. The value of I/N is thus given in terms of the experimentally determined curves by

$$I/N = B\,\nu'\,f(\nu')/\,P(\nu'). \qquad (4.7)$$

The equation may be equated to (4.4) and manipulated to provide

$$\alpha = C\,\nu'\,f(\nu')/\,P(\nu'). \qquad (4.8)$$

The terms B and C are constants, and the latter is adjusted by a scale factor to facilitate the graphical representation. The final result was further manipulated to present the function α as a function of wavelength rather than wave number. Both representations are common in the literature, but since much of the previous work on the present samples was reproduced as a function of wavelength, the present result is easier to compare in this representation. It is explicitly assumed that the signal voltage produced by the thermocouple was linear in incident power, and (τ/T_r) is assumed to be independent of the intensity of the radiation upon the specimen in the above derivation.

The Experimental Data

The spectral region from 5 to 40 μ failed to provide useful data even though the region corresponding to the 0.2 ev activation energy was carefully searched. The signal, if any, was always below the noise level. An indication of the relative density of the 0.2 ev to the 0.3 - 0.37 ev centers was reported to be about 10^{-3} (21). This would certainly make a 6 μ photoconductive maximum too weak to be observed in the present work. The wavelength range over which useful data were obtained at low crystal temperatures is 0.8 to 4.7 μ. Data obtained at shorter wavelengths were unreliable and are therefore not included. The uncorrected data do

not indicate that structure is present at the shorter wavelengths, but such a possibility cannot be ruled out.

The data obtained using specimen DS-2 are typical of all the data and are presented in Figs. 19 through 26. In each figure the plain solid curve represents the reduced data for the sample at 77°K, and the solid curve with dots identifies the 4.2°K data which were generally obtained soon after the 77°K data. The data shown in Figs. 19 through 24 were obtained on the IR-7, and the curves were normalized at 4.23 μ. The minor irregularities in the figures may be due to atmospheric absorption bands which were not entirely compensated by the experimental technique, but the gross features, including the relative minima near 3.5 and 3.62 μ, are features of the diamond.

Figures 21 through 24 were normalized at 3 μ and indicate the relative α from 2.6 to 3.5 μ obtained with the IR-7 system. The four sets of data show an interesting change which occurred in the curves with increased radiant flux upon the specimen. Figures 25 and 26 cover the spectral range from 0.8 to 2.7 μ. Figures 27 and 28 are reproduced because of an interesting distortion which appears in the response curve for the marquise cut specimen DS-3. The data shown in the last four figures were obtained on the DK-1 system.

The IR-7 Data

The relation between wavelength and energy, $\lambda \cdot E = 1.239\ \mu$ ev will be used to compare some of the features of the photoconductive data with results obtained by others. A graph of the relation is presented in Fig. 29 for wavelengths between 0.1 and 10 μ. The onset of the recorded photo-conductive signal is around 4.8 to 5 μ, but the first

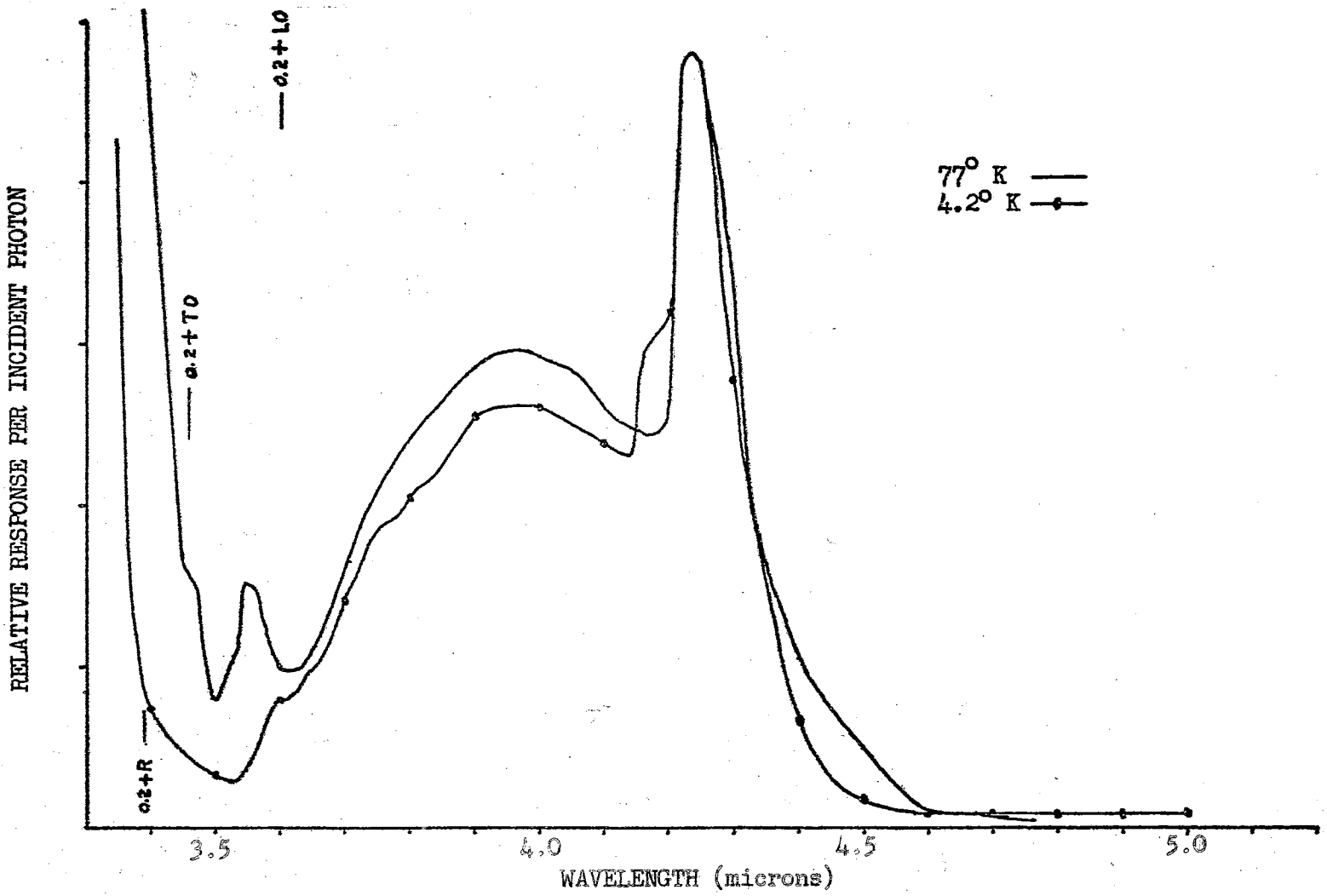

Fig. 19. Photoconductivity in diamond DS-2 using the IR-7 and a slit program providing a 4.2 mm slit at 4.16 μ.

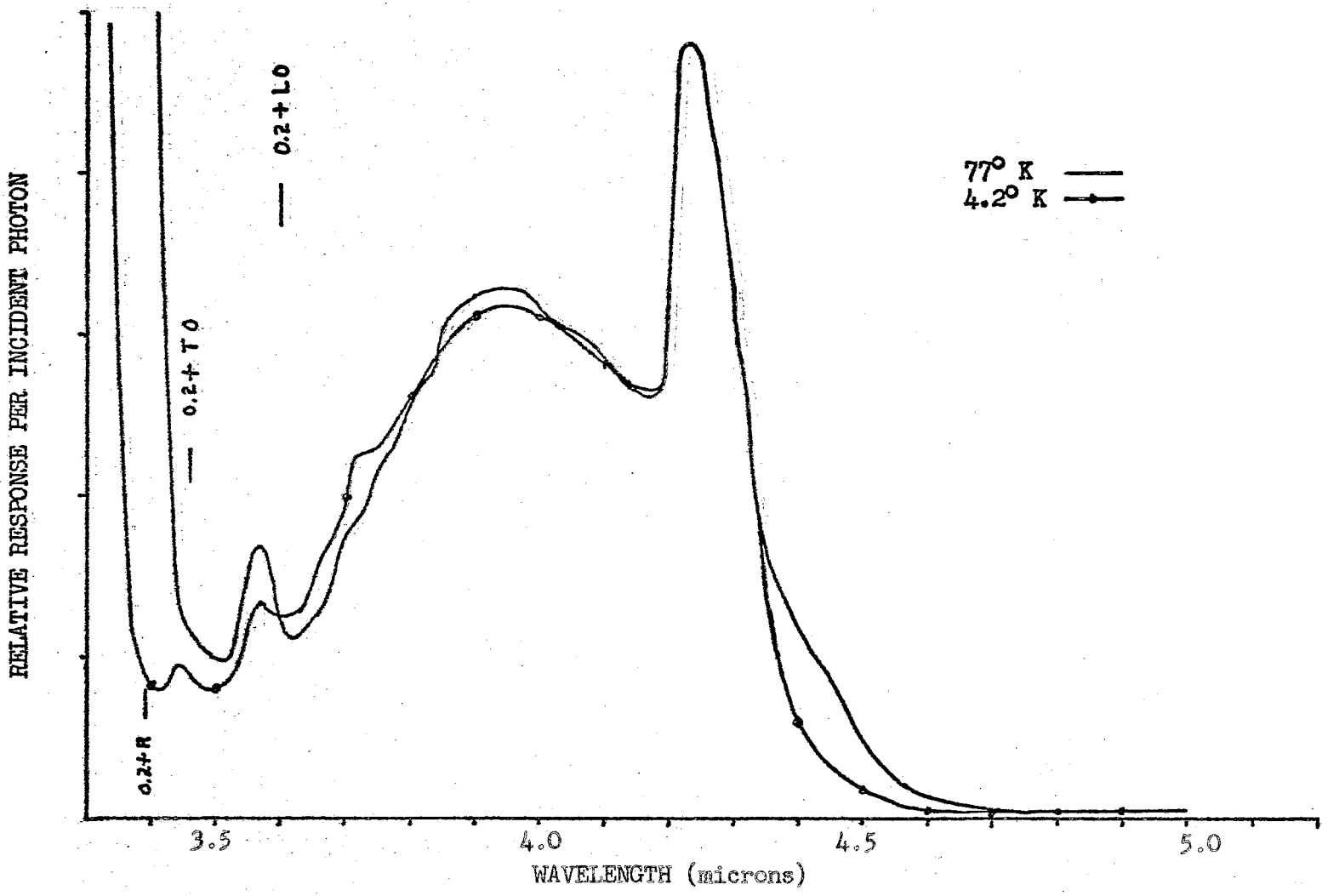

Fig. 20. Photoconductivity in diamond DS-2 using the IR-7 and a slit program providing a 4.5 mm slit at 4.16 μ.

steep increase in response begins at 4.6 μ (0.27 ev) for the 77°K data. The 4.2°K data show a sharp rise beginning near 4.45 μ, (0.278 ev), corresponding to a shift of about 0.009 ev.

The optical transmission data which were previously obtained on the same diamond show lattice absorption band which ranges from about 3.6 μ to about 4.2 μ with maximum absorption at 4.07 μ and a stronger region of absorption from about 4.2 to 5.8 μ with maxima near 4.6 and 5 μ (12). A transmission maximum between these regions of absorption appears nearly to coincide with the photoconductive maximum at 4.23 μ and the curves are quite similar from that wavelength to about 4.6 μ. Lattice competition for available photons is probably the cause of the shape of the long wavelength edge of the photoconductive curve as well as the large spike which appears at 4.23 μ. As previously mentioned the 4.23 μ photoconductive peak coincides with a CO_2 band in the atmosphere which should have been removed due to the way the data were recorded, and it should represent a feature of the diamond. The shape of the recorded photoconductive response curve including the 4.23 μ spike is probably a result of the competition of the lattice vibrations for the incident photons rather than an indication of the band shape which would result in the absence of such competition. The absorption constant associated with the 4.64 μ lattice peak was found by Charette (35) to decrease only 0.009/cm°K as the crystal was cooled from 0° to -200°C without a change in the frequency of the maximum or the form of the band. Charette's (36) investigation at 4.2°K does not provide the corresponding value for that temperature and does not display the transmission curves for this spectral region for comparison. From the work in this laboratory (12) there seems to be a slightly greater

transmission at 4.23μ at lower temperatures, but this is conjecture. The 0.3 ev activation energy and the optical absorption with maximum at 4.07μ , a characteristic of semiconducting diamonds, appear well correlated with the photoconductive data of Figs. 19 and 20.

Optical absorption maxima occur at 3.4 and 3.56μ (12). The low temperature study of Charette (35) indicates that the features responsible for these bands become sharper but do not change frequency as the crystal is cooled. The 3.56μ optical absorption peak coincides with a small peak in the photoconductivity which appears distinctly in three of the four curves of Figs. 19 and 20. The noise in the unreduced data probably caused the loss of the feature in the 4.2°K curve of Fig. 19. Structure which has been recorded in the infrared absorption is not apparent in the photoconductive response. It is interesting also to compare the absorption maxima recorded by Charette (35) for a semiconducting diamond at 4°K with the data of Fig. 20 corresponding to that temperature. Major optical absorption maxima appear at 3.61, 3.57, 3.56, and 3.43μ with many smaller features. The first of these wavelengths coincide with a photoconductive minimum, suggesting a competitive phenomenon whereas the 3.57 and 3.56μ peaks coincide with a photoconductive maximum. It is not clear in Fig. 19 if the 3.43μ absorption is competing with or contributing to photoconductivity. The sharp rise in the photoconductive curves near 3.4μ correlates well with a 0.37 ev activation energy. That energy corresponds to 3.35μ which is well within the edge of the band presented in the next four figures and the onset of photoionization in this range could obscure the competition near 3.4μ .

The next four figures, 21 through 24, provide the relative response corresponding to four slit programs on the IR-7. For Figs. 21 through

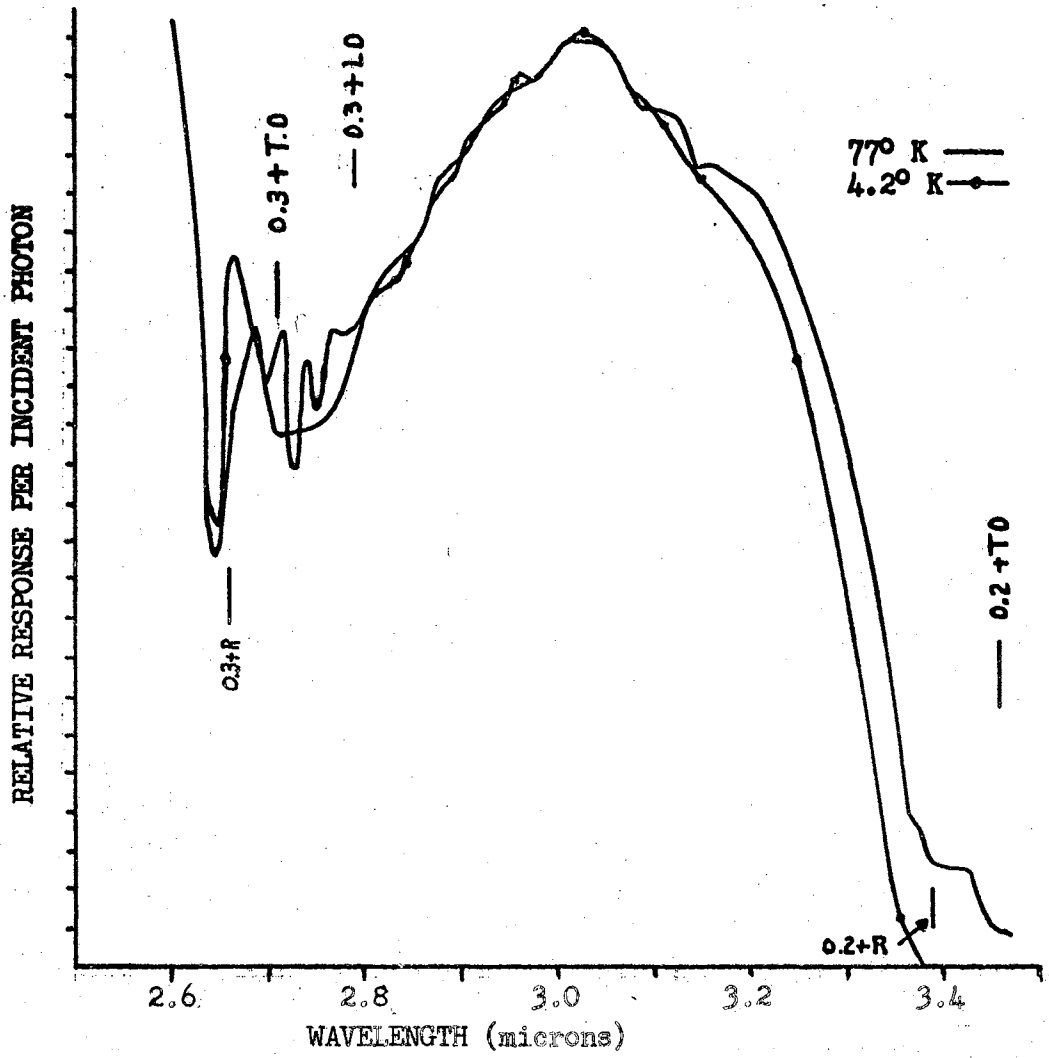

Fig. 21. Photoconductivity in diamond DS-2 using an IR-7 slit program providing a 1 mm slit at 3.23 μ.

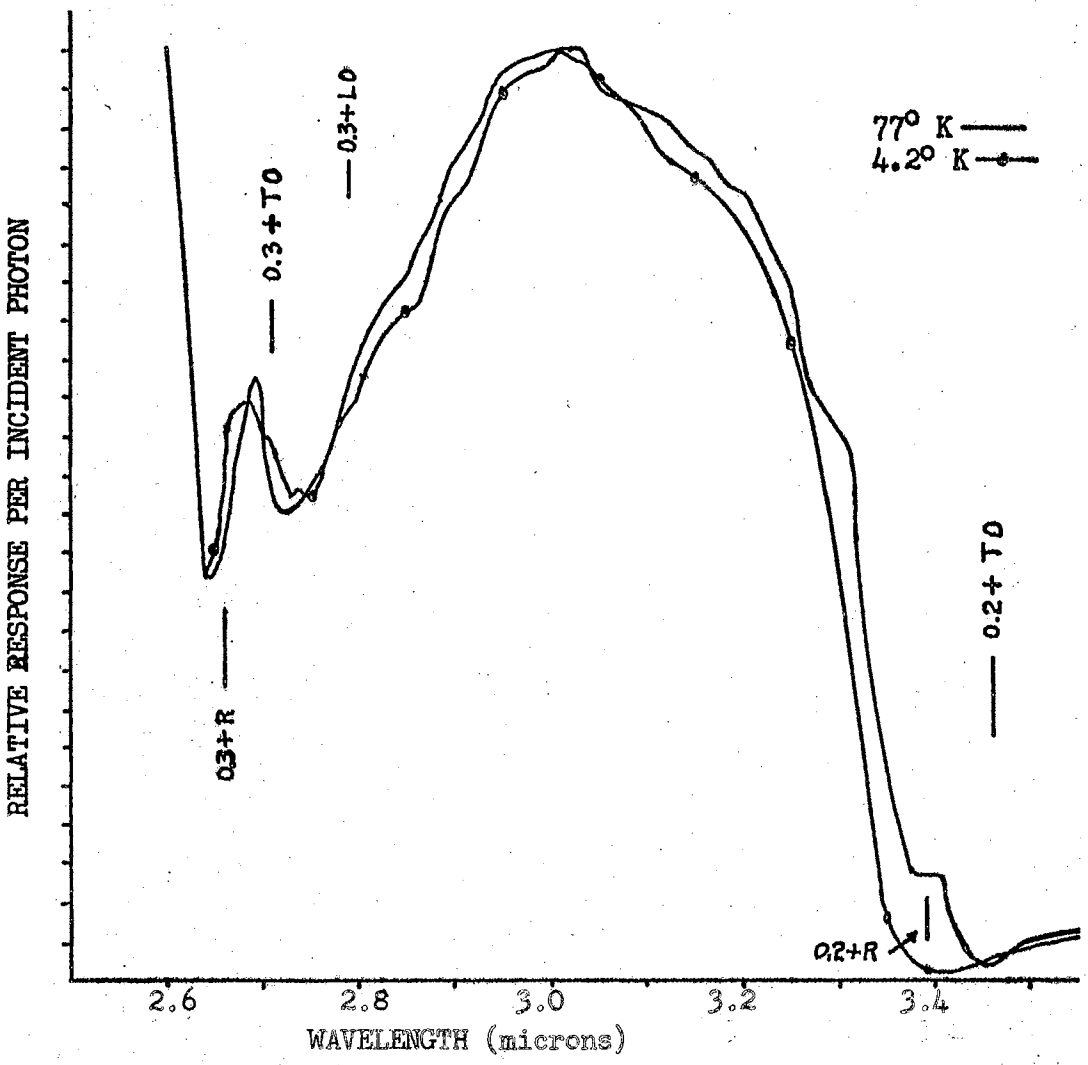

Fig. 22. Photoconductivity in diamond DS-2 using an IR-7 slit program providing a 1.57 mm slit at 3.23 μ.

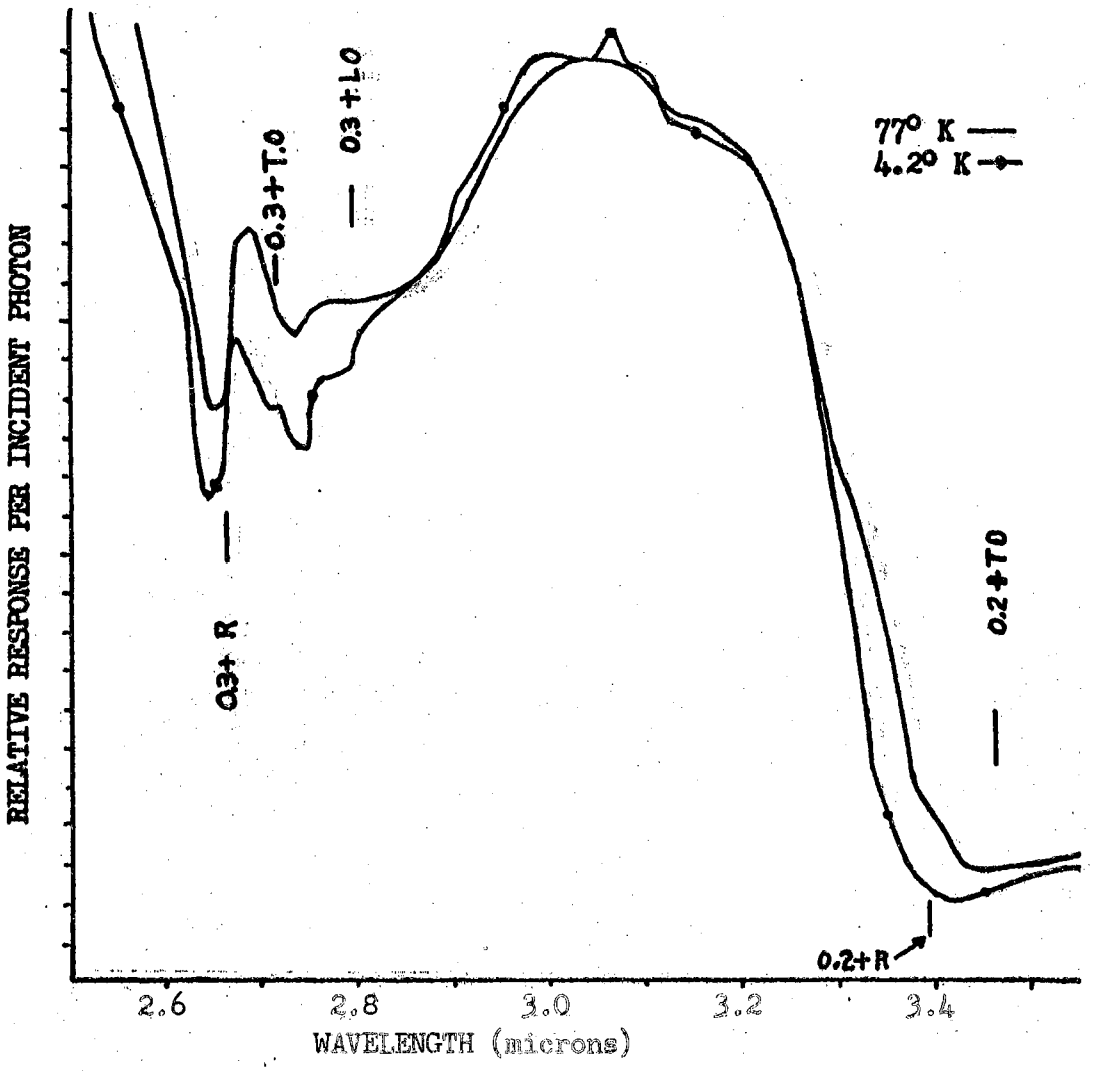

Fig. 23. Photoconductivity in diamond DS-2 using an IR-7 slit program providing a 2.5 mm slit at 3.23 μ.

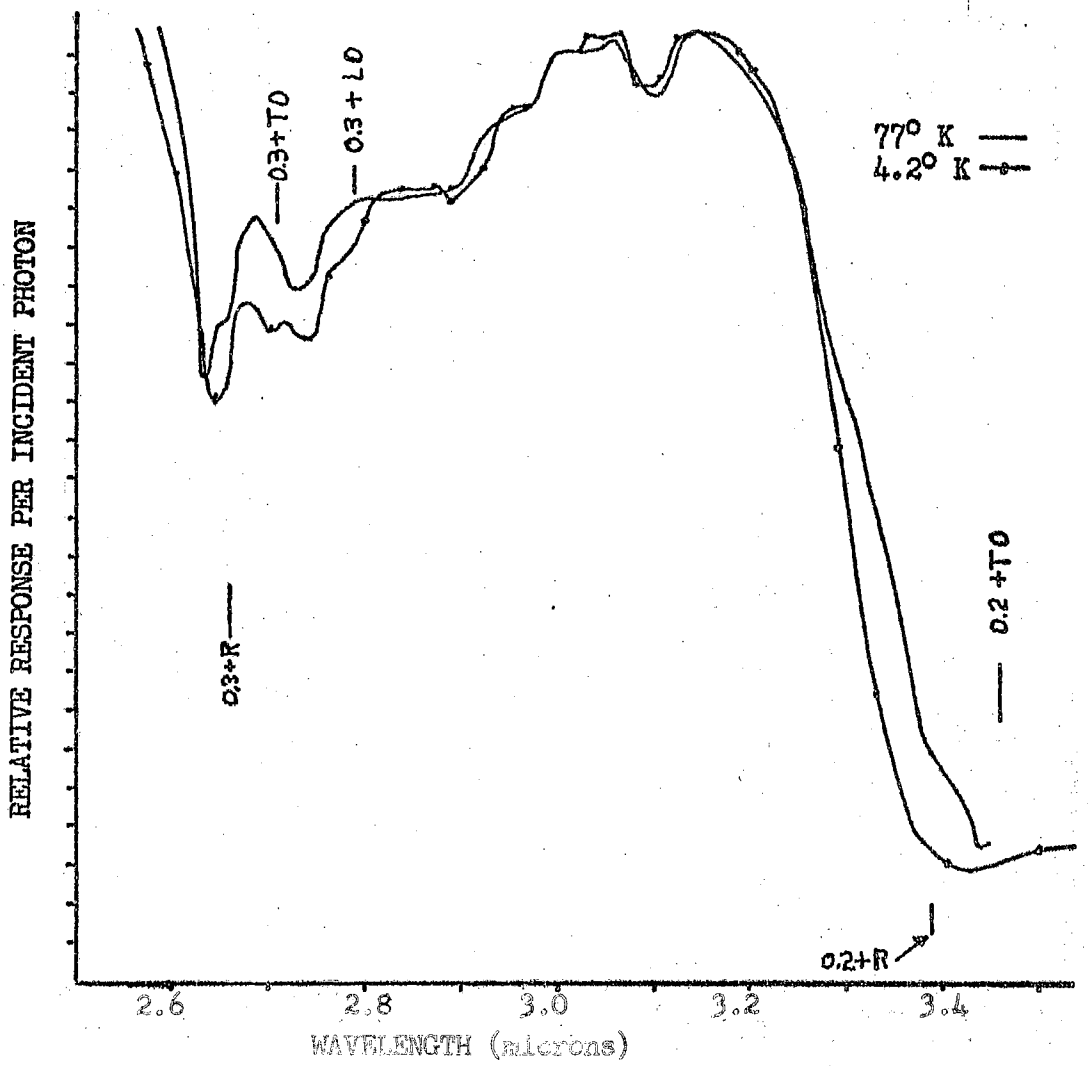

Fig. 24. Photoconductivity in diamond DS-2 using an IR-7 slit program providing a 3.2 mm slit at 3.23 μ.

24 the slit programs were in the ratios 1: 1.47; 2.5; 3.15. A gradual increase in the relative response at 3.15 μ (0.396 ev) with increasing slit width is quite apparent. The increased response is evidently temperature independent within the investigated range. The curves were normalized at 3.01 μ and therefore the response at that maximum does not change in the sequence of figures. Optical absorption maxima associated with the diamond lattice appear near 3.16 μ and 2.75 μ. The peak appearing at 3.15 μ in Fig. 24 may be related to a strong lattice coupling which aids in photoionization of the impurity centers. The 0.37 ev activation energy corresponds to 3.35 μ.

A feature at 3.4 μ in the 77°K data is missing from the 4.2°K data in Figs. 21 and 22 and is only suggested in the 77°K data in Figs. 23 and 24. In the latter figures the slit width is wide enough to cause the feature to be lost. This feature was also recorded in unreproduced data obtained with the DK-1 system. A calculation, using Fig. 20, of the energy difference between the sharp rise portion of the two curves near 3.4 μ yields 0.0082 ev. At the higher energy side of the photoconductive region of Figs. 21 through 24 two relative minima appear which are quite similar to the two in Figs. 19 and 20. The general shape of the bands in these two spectral regions is quite similar.

The DK-1 Data

The data of Fig. 25 covering the spectral region 1.75 to 2.7 μ reveal a photoconductive maximum from 2.5 to 2.55 μ and a broad minimum with structure from about 2.25 μ to 2.5 μ. From 1.75 μ to 2.35 μ the shape of the curve is similar to the two previous spectral regions. In the various optical absorption measurements mentioned earlier, an absorption maximum was found at 2.43 μ, and some investigators also

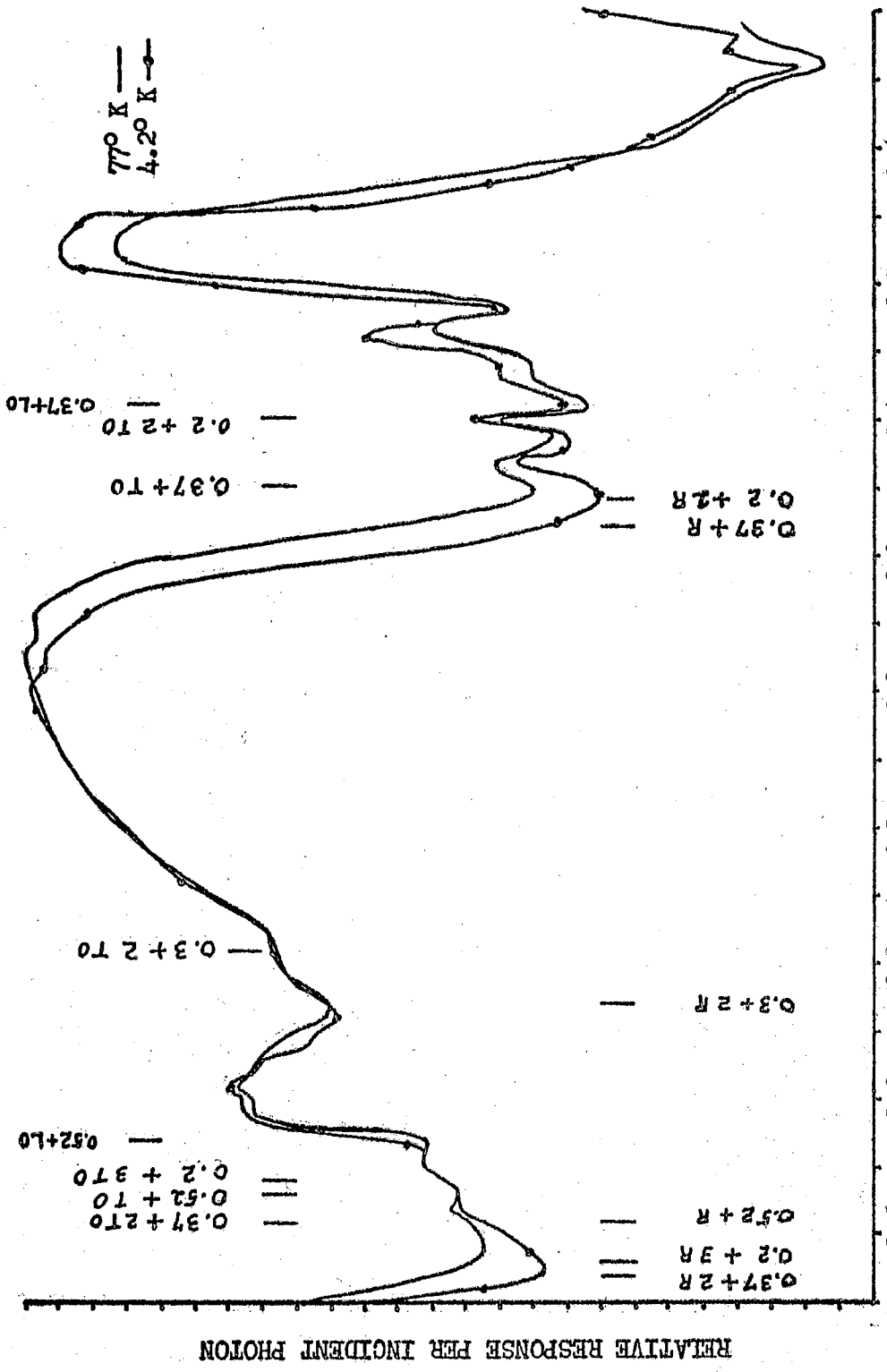

Fig. 25. Photoconductivity in DS-2 recorded with the DK-1 apparatus using a fixed 0.2 mm slit.

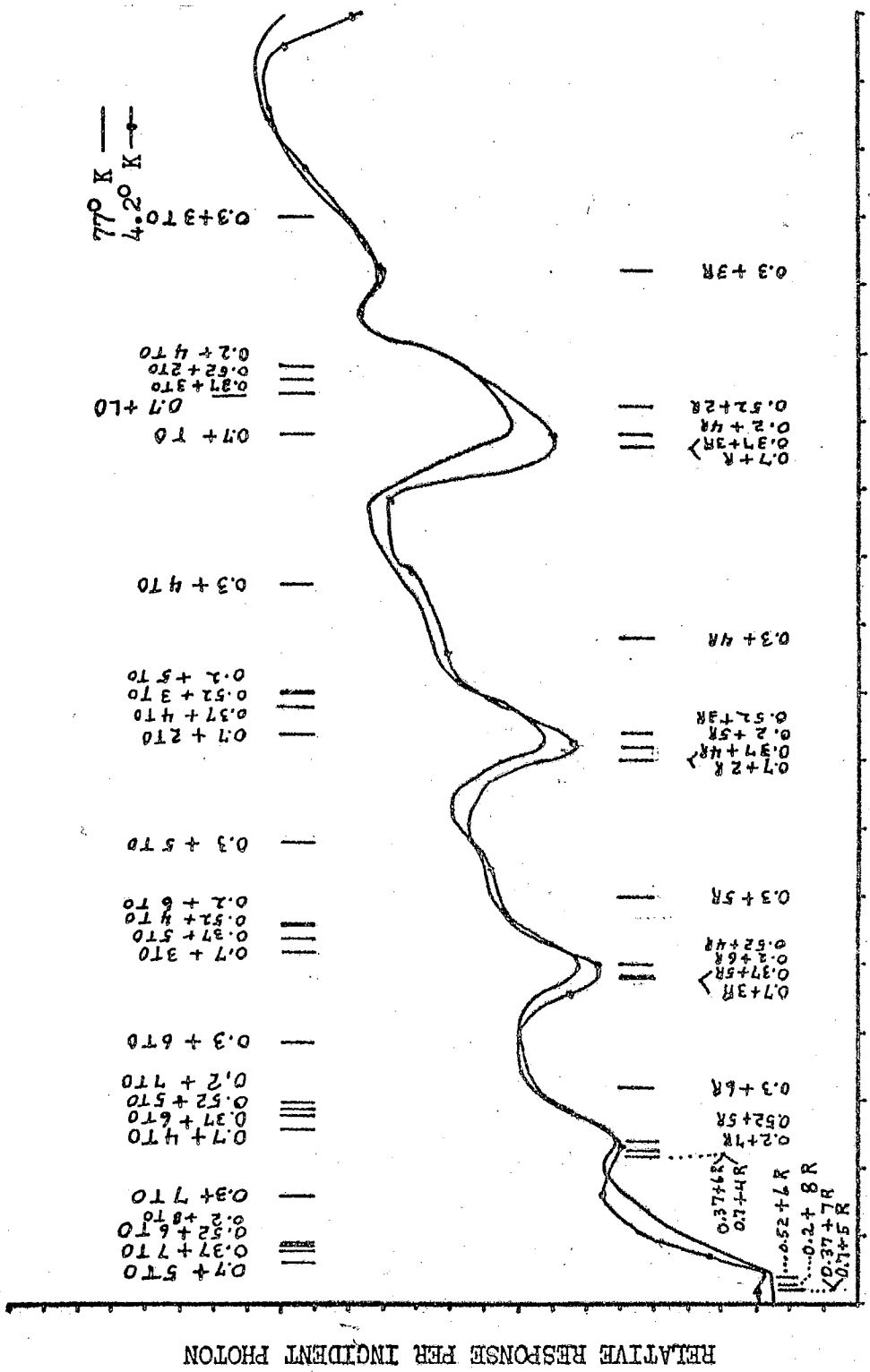

Fig. 26. Photoconductivity in DS-2 recorded with the DK-1 apparatus using a fixed 0.2 mm slit.

found a 2.35μ absorption maximum. Charette recorded, at a low temperature, a fine structure in the 2.43μ absorption. In particular he found relative absorption maxima at 2.45μ and 2.41μ. It is interesting to note that 2.35 and 2.41μ correspond to relative minima in the photoconductive response, and an inflection point appears at 2.44μ. There are also photoconductive minima at 2.38μ and 2.48μ. The value 2.43μ is nearly at the center of the broad photoconductive minimum which is not unlike the optical absorption recorded in this specimen at higher temperatures (12). A thermoluminescence activation energy of 0.52 ev (2.38μ) was found by Halperin and Nahun (21). This value falls in the broad relative photoconductive minimum rather than in a rising portion of the curve as one would expect. The competition from other crystal processes is believed to explain this distortion.

The photoconductivity beginning near 1.78μ in Fig. 25 passes through a maximum at about 1.72μ in Fig. 26. A thermoluminescence activation energy at 0.7 ev (1.77μ) appears to correspond with this increased photoconductivity (21). Six relative minima appear in the response curves between 1.7μ and 0.8μ. The only features which correspond to the photoconductive data obtained earlier on this specimen are relative maxima near 1.7 and 2.1μ.

Either the above features correspond to competing processes or each feature may be a new impurity center giving rise to a photoconductive band. Thermoluminescence or dark conductivity data would not have revealed such activation energies because the ionization energy is too high for thermal excitation to be significant at temperatures which would not damage the specimen. Minima due to competing processes may represent excitation to excited states of holes or possibly electrons

bound to crystal imperfections as mentioned above, or may result from phonon assisted transitions. If the former is the case, one would expect these features to appear in the optical absorption spectrum, but they do not appear. Kohn (54) has discussed shallow acceptor states in germanium and silicon. The effective mass theory is reasonably well justified in germanium for the "hydrogen atom" approximations of an impurity. The spin orbit splitting is only about 0.035 ev in silicon. Bloch waves associated with all six valence bands are involved with the acceptor wave functions. The theoretical treatment involves six coupled equations in silicon instead of the simpler case to which the germanium theoretical model reduces. The experimental result for acceptors in silicon indicates that the specific effect of each type of impurity is important. The ground state for each acceptor is different, and the excited states may not be hydrogen-like. In view of the above effect in the change from germanium to silicon, one should expect distinct ground states for various imperfections in diamond. The diamond crystals are natural specimens containing unknown quantities of imperfections. The precise knowledge and control of impurities possible in the study of germanium and silicon is not presently possible in diamond.

In the DK-1 data for the blue marquise cut semiconducting diamond DS-3, a striking increase in response with increasing photon energy was noted. For this reason the data were reduced and are graphed in Figs. 27 and 28. The structure is the same as that in the data for DS-2, except for the gradual rise in the overall response. It is believed that the effect was caused by the approach of critical reflecting angles inside the specimen with decreasing wavelength which caused a continually increasing optical path length. The portion of the graph on the left

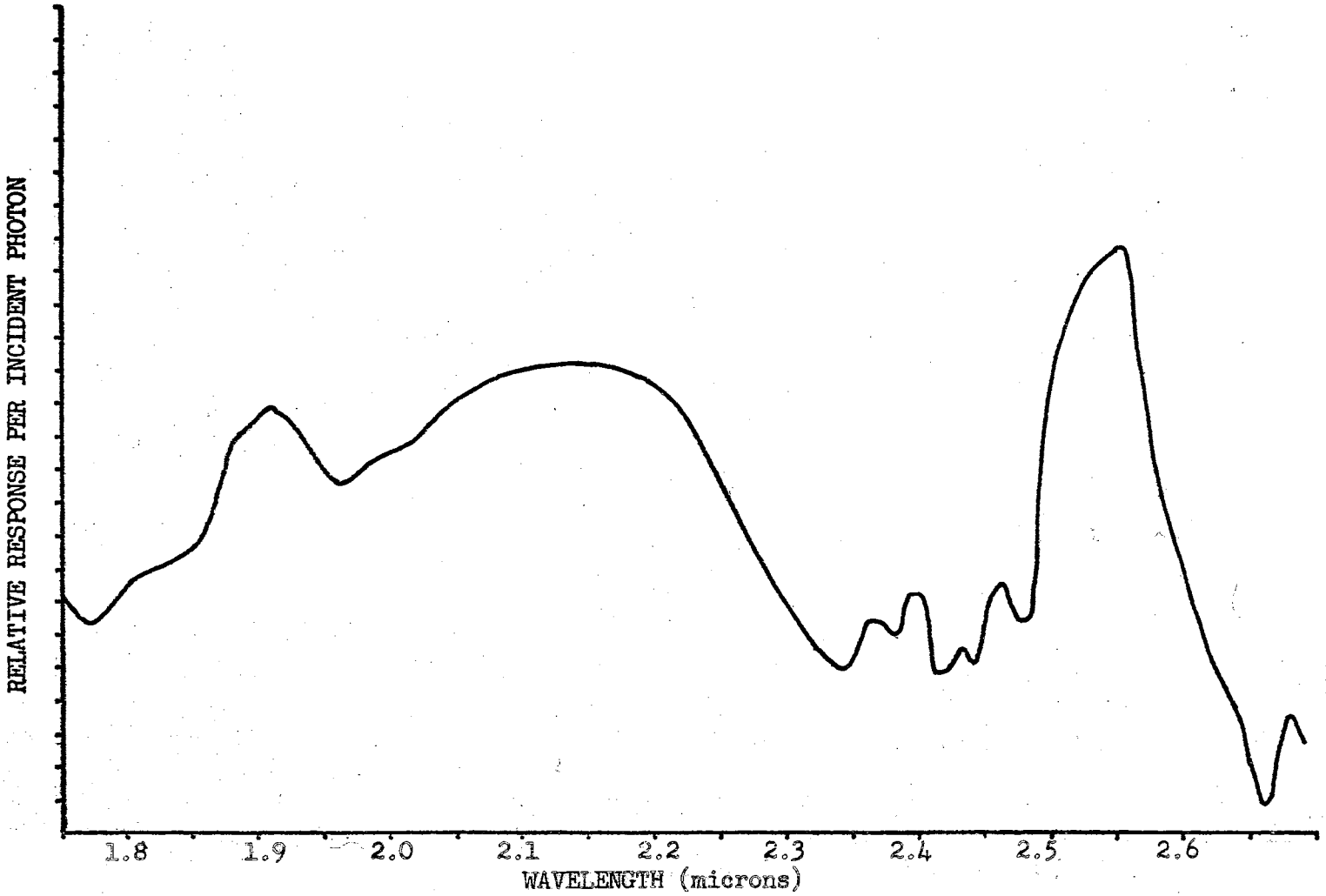

Fig. 27. Photoconductivity in DS-3 at 4.2°K.

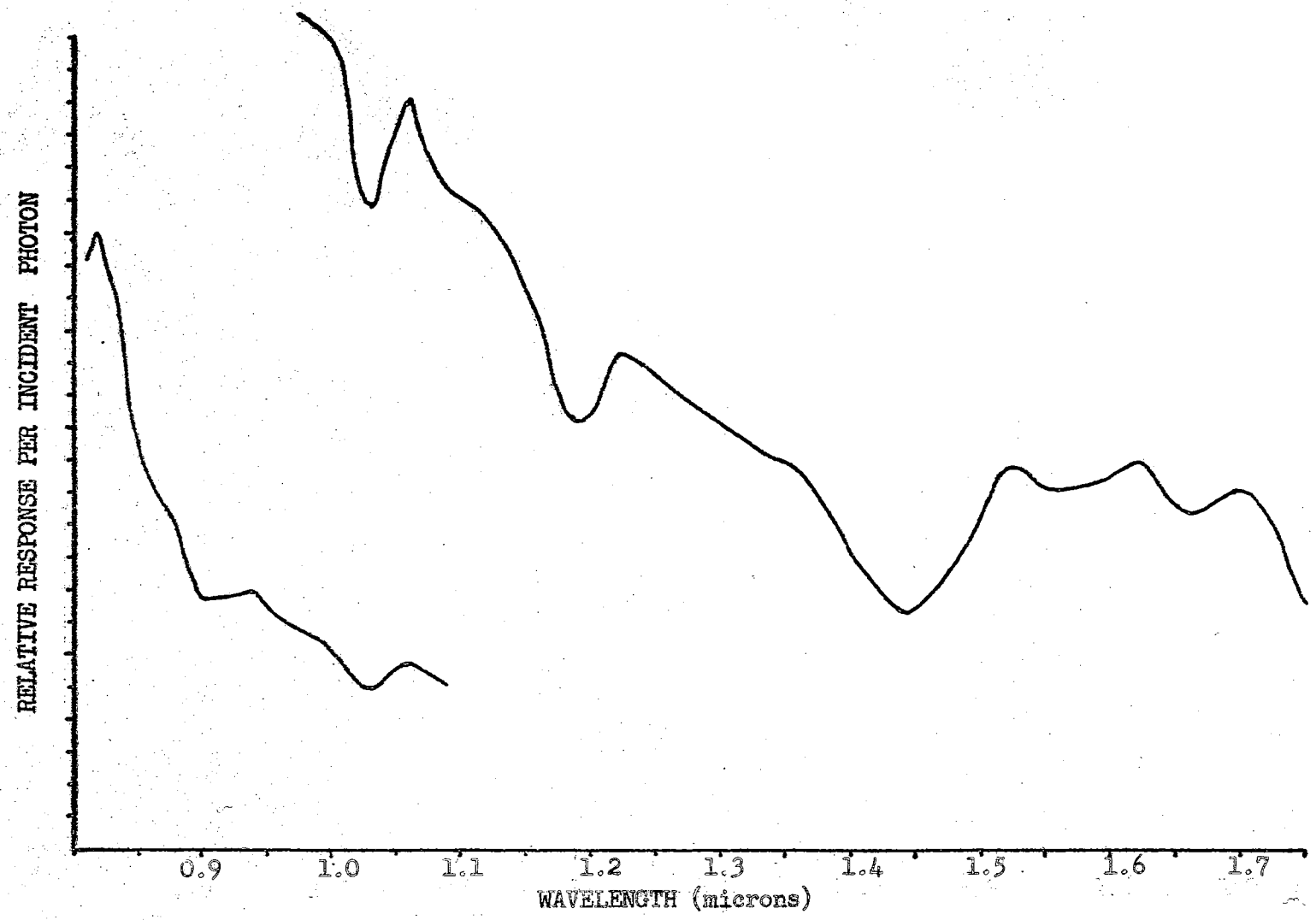

Fig. 28. Photoconductivity in DS-3 at 4.2° K.

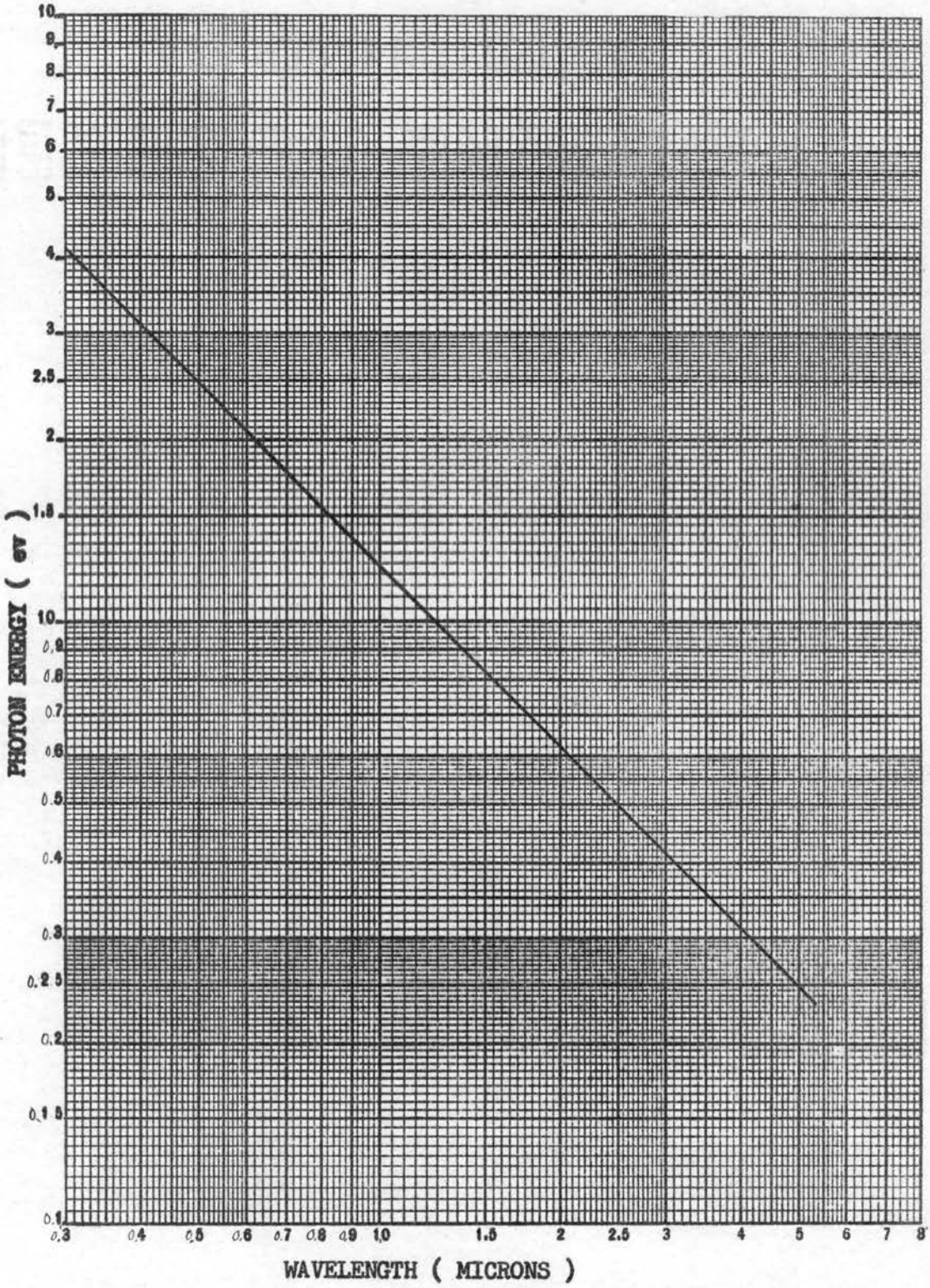

Fig. 29. A graph for conversion between wavelengths in microns and energy in electron volts

side of Fig. 28 should be multiplied by a factor of four to place it in proper perspective. The rest of the data on the other samples appeared to be the same as that presented here, and the tedious job of reducing them was not undertaken.

Conclusions

The photoconductive response obtained in the present work appears to support the various activation energies for semiconducting diamond which have been found by other workers. These energies are approximately 0.2, 0.3, 0.37, 0.52 and 0.7 ev. When allowance is made for competition from crystal processes not giving rise to photoconductivity the present data correspond well with the largest four of the five energies listed above.

At low temperatures many shallow acceptors may be ionized due to compensation. It is believed that the relatively small density of un-ionized 0.2 ev centers and competition for photons by lattice absorption cause any associated photoconductivity to be of very small magnitude and explain why no corresponding signal was recorded. Lattice absorption is believed also to cause the sharp peak in the photoconductive response curves of Figs. 19 and 20. The present photoconductive data suggest lattice assistance to photoionization at 3.15 μ with increasing radiant flux upon the diamond, because a distinctly new peak appears at that wavelength in Fig. 24.

The photoconductive curve of Fig. 25 has the shape of the optical transmission curve from 2.45 to 2.6 μ and apparently it only indicates the relative number of photons available for photoionization. The 0.52 ev (2.38 μ) activation energy does not coincide with a rise in the

photoconductive response, but this is believed to be due to competition from phonon interactions to be discussed below. The 0.7 ev (1.77 μ) activation energy appears to correspond with a photoconductive rise if similar phonon competition is recognized.

The optical absorption curves show none of the structure which appears in the present photoconductive data at wavelengths less than 2 μ. The structure is believed to be due to competition from optical phonons. Rauch (30, 31) and Hardy, Smith, and Taylor (29) have observed phonon competition in the photoconductivity of semiconducting diamond, and Engler, Levinstein and Stannard (55) recorded an oscillatory photoresponse in indium antimonide. The interpretation was different in these reports.

Hardy, Smith, and Taylor made use of only the 0.35 ev activation energy and excited states of this center at 0.304, 0.343, and 0.363 ev in interpreting their photoconductivity. The present work records photoconductivity over a greater spectral range at liquid helium as well as liquid nitrogen temperature and, as was mentioned above, it supports a model with several acceptors of different energies. In addition, present work indicates that both T.O. phonons and the 0.165 ev phonon corresponding to the Raman scattering energy are effective in competing with photoconductivity in semiconducting diamonds. Phonons in the optical branch are exceedingly dense at energies 0.165, 0.158, and 0.144 ev, at which values the dispersion curves are flat. If in the photon absorption process the hole at an acceptor is excited with zero velocity, the extra energy having created optical mode phonons, the hole may be trapped into an excited state at an ionized acceptor (some of which always occur due to compensation by donors) and decay to the ground state.

This process would compete with the photoconductive response. Hardy, Smith and Taylor conclude, after a theoretical analysis, that for the optical branches one expects phonon emission peaks to occur at multiple phonon energies above any direct transition of energy with intensity inversely related to the number of phonons emitted.

Tables III and IV each show the five activation energies (and wavelengths) listed above as well as a series of energies (and wavelengths) formed by adding integral multiples of the important phonon energies to the activation energies. The resulting wavelengths are marked on the data curves of Figs. 20 through 26. The series for 0.165 ev phonons are marked below the photoconductive response curves and the T. O. and some L. O. phonon combinations are marked above. There is a striking correspondence between (a) the minima in the photoconductive curves and clusters of 0.165 ev interactions, and (b) the general shape of the minima and the density and location of all phonon interactions. The effect appears reduced for greater numbers of phonons, but a distinct correlation is recorded for up to eight 0.165 ev phonons.

The L. O. mode phonon (0.144 ev) series corresponds with photoconductive minima only for one phonon. For two or more the correspondence is generally poor except for the series beginning at 0.37 ev.

The present work agrees with a statement by Rauch that the competition associated with energy near .3 ev is less severe than other competition. In the present work this seems to be due to the fortuitous clustering of the other four activation energies which places as many as 8 competing processes in one absorption feature. It seems that the best explanation of the large number of minima in the photoconductive response curves is given in terms of competition due to phonon interactions.

TABLE III

MULTIPLES OF RAMAN ENERGY PHONONS BEGINNING AT THE IMPURITY IONIZATION ENERGIES

Imperfection Center	E_i + N (0.165) ev								
	N = 0	1	2	3	4	5	6	7	8
E_i (ev)	0.20	0.365	0.530	0.695	0.860	1.025	1.190	1.355	1.520
(microns)	6.20	3.39	2.34	1.78	1.44	1.21	1.04	0.914	0.815
	0.30	0.465	0.630	0.795	0.960	1.125	1.290		
	4.13	2.66	1.97	1.56	1.29	1.10	0.960		
	0.37	0.535	0.700	0.865	1.030	1.195	1.360	1.525	1.690
	3.35	2.32	1.77	1.43	1.20	1.04	0.911	0.812	0.733
	0.52	0.685	0.850	1.015	1.180	1.345	1.510	1.675	
	2.38	1.81	1.46	1.22	1.05	0.921	0.821	0.740	
	0.70	0.865	1.030	1.195	1.360	1.525	1.690		
	1.77	1.43	1.20	1.04	0.911	0.812	0.733		

TABLE IV

MULTIPLES OF PHONONS BEGINNING AT THE IMPURITY IONIZATION ENERGIES

	T O PHONONS								L O PHONONS
Imperfection Center	E_i + N (0.158) ev								E_i+0.144 ev
	N = 0	1	2	3	4	5	6	7	
E_i (ev)	0.20	0.358	0.516	0.674	0.832	0.990	1.148	1.306	0.344
λ (microns)	6.20	3.46	2.40	1.84	1.49	1.25	1.08	0.949	3.60
	0.30	0.458	0.616	0.774	0.932	1.090	1.248	1.406	0.444
	4.13	2.71	2.01	1.60	1.33	1.14	0.993	0.881	2.79
	0.37	0.528	0.686	0.844	1.002	1.160	1.318	1.476	0.514
	3.35	2.35	1.81	1.47	1.24	1.07	0.94	0.84	2.41
	0.52	0.678	0.836	0.994	1.152	1.310	1.468	1.626	0.664
	2.38	1.83	1.48	1.25	1.08	0.945	0.844	0.762	1.87
	0.70	0.858	1.016	1.174	1.332	1.490	1.648	1.806	0.844
	1.77	1.44	1.22	1.06	0.930	0.832	0.752	0.686	1.468

Suggestions for Further Study

The problem of making an ohmic contact to the diamond is significant. The noise level due to contacts seriously limited the experiment and made it impossible to find the anticipated photoconductive signal near 6 μ. The visible region might be covered more completely also.

The uncertainty caused by atmospheric absorption could be eliminated by a complete purge of the ambient or perhaps by designing a system to operate in a reduced pressure so that water and carbon dioxide bands would not appear in the background.

It would help significantly in the visible region of the spectrum if a stronger source of radiation of 0.4 to 0.9 μ wavelength were available. More radiation and better contacts would allow extension of the data to the 0.44 μ wavelength which is of interest due to the previously recorded photovoltaic effect.

Finally it would be of immense help in reducing the data to its most meaningful form if a ratio recording system could be used so that the photosignal could be continuously compared with the incident energy and the point by point use of equation (4.8) would not be necessary. Such an apparatus could be used in various other experiments also.

BIBLIOGRAPHY

1. C. Kittel, Introduction to Solid State Physics (John Wiley and Sons, Inc., New York, 1957) 2nd ed.

2. W. A. Wooster, A Textbook on Crystal Physics (Cambridge University Press, 1949).

3. W. Shockley, Electrons and Holes in Semiconductors (D. Van Nostrand Co., Inc., New York, 1956).

4. R. Robertson, J. J. Fox, and A. E. Martin, "Two Types of Diamond," Phil. Trans. Roy. Soc. London 232, 463 (1934).

5. R. Robertson, J. J. Fox, and A. E. Martin, "Further Work on Two Types of Diamond," Proc. Roy. Soc. (London) A157, 579 (1936).

6. J. F. H. Custers, "Unusual Phosphorescence of a Diamond," Physica 18, 489 (1952).

7. J. F. H. Custers, "Type IIb Diamonds," Physica 20, 183 (1954).

8. W. J. Leivo and R. Smoluchowski, "A Semiconducting Diamond," Phys. Rev. 98, 1532 (1955).

9. J. J. Brophy, "Preliminary Study of the Electrical Properties of Semiconducting Diamond," Phys. Rev. 99, 1336 (1955).

10. H. J. Stein, M. D. Bell, and W. J. Leivo, "Optical Studies on Semiconducting Diamonds," Bull. Am. Phys. Soc. 1, 127 (1956).

11. W. J. Leivo, et al, "Investigation of Semiconducting Properties of Type IIb Diamonds," Report No. AFOSR-2642, (May, 1962).

12. C. Johnson, H. Stein, T. Young, J. Wayland and W. J. Leivo, "Photoeffects and Related Properties of Semiconducting Diamonds," J. Phys. Chem. Solids 25, 827 (1964).

13. I. G. Austin and R. Wolfe, "Electrical and Optical Properties of Semiconducting Diamond," Proc. Phys. Soc. (London) B69, 329 (1956).

14. C. D. Clark, R. W. Ditchburn, and H. B. Dyer, "The Absorption Spectra of Natural and Irradiated Diamonds," Proc. Roy. Soc. A234, 363 (1956).

15. M. D. Bell and W. J. Leivo, "Rectification, Photoconductivity and Photovoltaic Effect in Semiconducting Diamond," Phys. Rev. 111, 1227 (1958).

16. C. C. Johnson, and W. J. Leivo, "Photoconductivity in Semiconducting Diamonds" Bull. Am. Phys. Soc. 3, 11 (1958).

17. J. H. Wayland and W. J. Leivo, "Lifetimes and Trapping of Carriers in Semiconducting Diamonds," Bull. Am. Phys. Soc. 3, 400 (1958).

18. J. B. Krumme, and W. J. Leivo, "Luminescence in Semiconducting Diamonds," Bull. Am. Phys. Soc. 5, 187 (1960).

19. M. D. Bell, and W. J. Leivo, "Electron Spin Resonance in Semiconducting Diamond," Bull. Am. Phys. Soc. 6, 142 (1961).

20. M. D. Bell, "Electron Spin Resonance in Diamond," Doctoral Thesis, Oklahoma State University, Stillwater, Oklahoma, 1964.

21. A. Halperin, and J. Nahum, "Some Optical and Electrical Properties of Semiconducting Diamonds," J. Phys. Chem. Solids 18, 297 (1961).

22. R. Wolfe, and J. Woods, "Electroluminescence of Semiconducting Diamonds," Phys. Rev. 105, 921 (1957).

23. J. C. Male, "Luminescence Excitation Spectrum of Diamond near the Fundamental Absorption Edge," Proc. Phys. Soc. 77, 869 (1961).

24. J. C. Male and J. R. Prior, "Intrinsic Recombination Radiation in Diamond," Nature 186, 1037 (1960).

25. R. J. Collins and H. Y. Fan, "Infrared Lattice Absorption Bands in Germanium, Silicon and Diamond," Phys. Rev. 93, 674 (1954).

26. K. Lonsdale, Acta Cryst. 1, 142 (1948).

27. M. Lax and E. Burstein, "Infrared Lattice Absorption in Ionic and Homopolar Crystals," Phys. Rev. 97, 39 (1955).

28. J. R. Hardy and S. D. Smith, "Two-phonon Infrared Lattice Absorption in Diamond," Phil. Mag. 6, 1163 (1961).

29. J. R. Hardy, S. D. Smith, and W. Taylor, "Optical Phonon Effects in Absorption and Photoconductivity of Semiconducting Diamond," Proceedings of the International Conference of The Physics of Semiconductors, Exeter, July, 1962.

30. C. J. Rauch, "Millimeter Cyclotron Resonance Experiments in Diamond," Phys. Rev. Letters 7, 83 (1961).

31. C. J. Rauch, "Millimeter Cyclotron Resonance in Diamond," Proceedings of the International Conference of The Physics of Semiconductors, Exeter, July, 1962.

32. A. G. Redfield, "Electronic Hall Effect in Diamond" Phys. Rev. 94, 526 (1954).

33. J. L. Birman, "Theory of Infrared and Raman Processes in Crystals: Selection Rules in Diamond and Zincblende," Phys. Rev. 131, 1489 (1963).

34. R. Mykolajewycz, J. Kalnajs, and A. Smakula, "High-Precision Density Determination of Natural Diamonds," J. Appl. Phys. 35, 1773 (1964).

35. J. J. Charette, "Le Spectre Infra-Rouge A. Grande Disperson Des Trois Types De Diamants Et Ses Variations En Fonction De La Temperature," Physica 25, 1303 (1959).

36. J. J. Charette, "Essai De Classification Des Bandes D'Absorption Infra-Rouge Du Diamont," Physica 27, 1061 (1961).

37. W. Smith, Nature 7, 303 (1873).

38. R. H. Bube, Photoconductivity of Solids (John Wiley and Sons, Inc., New York, 1960).

39. A. Rose, "Concepts in Photoconductivity and Allied Problems"(John Wiley and Sons, Inc., New York, 1963).

40. A. Rose, "Performance of Photoconductors," Proc. IRE 43, 1850 (1955).

41. N. F. Mott and H. Jones, The Theory of the Properties of Metals and Alloys (Dover Publications, Inc., New York, 1958).

42. A. J. Dekker, Solid State Physics (Prentice-Hall, Inc., Englewood Cliffs, New Jersey, 1957).

43. P. J. Dean, and I. H. Jones, "Recombination Radiation from Diamond," Phys. Rev. 133, A1698 (1964).

44. S. Whitehead and W. Hackett, "Measurement of the Specific Inductive Capacity of Diamonds," Proc. Phys. Soc. (London) 51, 173 (1939).

45. J. S. Blakemore, Semiconductor Statistics, (Pergamon Press, New York, 1962).

46. R. C. Jones, "Noise in Radiation Detectors," Proc. IRE 47, 1481 (1959).

47. P. Grodzinski, "Diamond Technology" (Huebner Pub., Inc., Cleveland, Ohio, 1954) 2nd ed.

48. S. Seely, Election Tube Circuits (McGraw Hill Book Co., Inc., New York, 1958).

49. J. R. MacDonald, Rev. Sci. Instr. 25, 144 (1954).

50. R. B. Scott, Cryogenic Engineering (D. Van Nostrand Co., Inc., Princeton, New Jersey, 1959).

51. G. K. White, Experimental Techniques in Low-Temperature Physics (Oxford University Press, London, 1959).

52. L. J. Schoen and H. P. Broida, "Glass Dewars for Optical and Other Studies at Low Temperatures," Rev. Sci. Instr. 33, 470 (1962).

53. R. L. Powell, M. D. Bunch, and R. J. Corruccini, "Low Temperature Thermocouples-1, Gold-Cobalt or Constantan vs Copper or 'Normal' Silver," Cryogenics 1, 139 (1961).

54. W. Kohn, "Shallow Impurity States in Silicon and Germanium," Solid State Physics Vol. 5 (Academic Press, Inc., New York, 1957), p 258.

55. W. Engeler, H. Levinstein, and C. Stannard, Jr., "Photoconductivity in p-type Indium Antimonide with Deep Acceptor Impurities," J. Phys. Chem. Solids 22, 249 (1961).

VITA

Jefferson Bryan Krumme

Candidate for the Degree of

Doctor of Philosophy

Thesis: PHOTOCONDUCTIVITY IN SEMICONDUCTING DIAMONDS AT LOW TEMPERATURES

Major Field: Physics

Biographical:

Personal data: Born in Tuskegee, Oklahoma, July 14, 1924, the son of Roy and Ruth Krumme.

Education: Attended elementary and secondary school at Bristow, Oklahoma and was graduated from Bristow High School in May, 1942; received Bachelor of Science degree from Oklahoma State University, with a Major in Physics, in May 1958; received the Master of Science degree from Oklahoma State University with a Major in Physics, in August 1960; completed requirements for the Doctor of Philosophy degree in January 1965.

Experience: Served in U. S. Army during World War II; operated private business for ten years.

Organizations: Member of American Physical Society, Sigma Pi Sigma, Pi Mu Epsilon, Phi Kappa Phi, Oklahoma Academy of Sciences, and Associate Member of Sigma Xi.